ELSEVIER

International Journal of Mass Spectrometry 218 (2002) 105–130

International Journal of Mass Spectrometry

www.elsevier.com/locate/ijms

Review

Advanced integrated stationary afterglow method for experimental study of recombination of processes of H_3^+ and D_3^+ ions with electrons

R. Plašil, J. Glosík*, V. Poterya, P. Kudrna, J. Rusz, M. Tichý, A. Pysanenko

Department of Electronics and Vacuum Physics, Faculty of Mathematics and Physics, Charles University Prague, V Holšovckách 2, Prague 8, Czech Republic

Received 22 February 2002; accepted 13 May 2002

Abstract

The study of the recombination of H_3^+ and D_3^+ ions with electrons, with detailed description of the method and new experimental instrument—the advanced integrated stationary afterglow (AISA), is reported. In the stationary afterglow in He–Ar–H_2 and He–Ar–D_2 mixtures was observed that the recombination of H_3^+ and D_3^+ ions are three-body processes with the rate coefficients dependent on the partial density of [H_2] and [D_2], respectively. These results obtained at [H_2] and [D_2] below 1×10^{11} cm^{-3} indicate that the binary dissociative recombination reactions of H_3^+ and D_3^+ ions with electrons are, at thermal energies, very slow processes with rate coefficients smaller than 3×10^{-9} cm^3 s^{-1} and 6×10^{-9} cm^3 s^{-1}, respectively. (Int J Mass Spectrom 218 (2002) 105–130)

Keywords: Recombination; H_3^+; D_3^+; Interstellar ions; Stationary afterglow; Plasma

1. Introduction

H_3^+ ions are the starting point in the formation of more complex ions in interstellar clouds via ion–molecule reactions [1–8]. H_3^+ ions are also important in ion chemistry in atmospheres of large planets [3,9,10]. The importance of these ions in interstellar medium was emphasised on the discussion meeting of the Royal Society on "*Astronomy, Physics and Chemistry of* H_3^+" in London (2000) and on 222nd National ACS Meeting in Chicago (2001), see, e.g. [11–15]. H_3^+, H_2D^+, HD_2^+ and D_3^+ ions also play important role in many terrestrial plasmas (discharges, fusion plasmas at walls [16] etc.). In the following description of experiment and general discussions, H_3^+ will be used to refer both H_3^+ and D_3^+ ions, as long as it will not lead to confusion.

The kinetics of the formation of H_3^+, H_2D^+, HD_2^+ and D_3^+ ions in interstellar environment is well understood and also kinetics and dynamics of reactions of this ion with neutral atoms and molecules is known and was described in many reviews and compilations of rate coefficients [17–19]. It is also known that the kinetics and dynamics of the three-body association

* Corresponding author. E-mail: radek.plasil@mff.cuni.cz

1387-3806/02/$ – see front matter
PII S1387-3806(02)00714-5

of this ion in high pressure and low temperature environment [17,20–22]. The critical point in modelling of hydrogen containing plasmas, including interstellar plasma and ionosphere of planets, is the recombination of H_3^+ and its deuterated analogues with electrons. H_3^+ and D_3^+ ions are simple three-atomic ions comparatively easy to theoretical treatment (see, e.g. [23] and references therein). One would not therefore anticipate problems in determination of the rate coefficient for the recombination reaction of these ions with electrons. The reality is, however, different.

In the very early laboratory studies half a century ago (1949) Biondi and Brown [24] obtained the recombination rate coefficient $\alpha = 2.5 \times 10^{-6}\,\mathrm{cm^3\,s^{-1}}$ in the stationary afterglow (SA) in H_2. This study was followed by study of Richardson and Holt [25] with $\alpha \approx 6 \times 10^{-6}\,\mathrm{cm^3\,s^{-1}}$ and by Varnerin [26] with $\alpha \approx 3 \times 10^{-7}\,\mathrm{cm^3\,s^{-1}}$. Persson and Brown in 1955 carried out measurements [27] in high purity stationary afterglow and they obtained very low value of the recombination coefficient $\alpha = 3 \times 10^{-8}\,\mathrm{cm^3\,s^{-1}}$. Later in seventies several experiments were carried out that yielded the recombination rate coefficient α of the order 2×10^{-7} to $3 \times 10^{-7}\,\mathrm{cm^3\,s^{-1}}$ at 300 K. However, in 1984 Adams et al. [28] obtained in FALP apparatus the recombination rate for this reaction $\alpha_H \approx 2 \times 10^{-8}\,\mathrm{cm^3\,s^{-1}}$. This result supported theoretical predictions indicating unfavourable curve crossing between the ion ground state and the dissociating neutral state (see, e.g. [29] and references therein). Later on Amano in 1990 [30], using an infrared spectroscopic absorption technique in stationary afterglow, obtained $\alpha = 1.8 \times 10^{-7}\,\mathrm{cm^3\,s^{-1}}$ at 273 K. Important was that Amano specified the vibrational state of recombining ions, namely as ground state ions, $H_3^+(v = 0)$. In order to solve this discrepancy, new FALP apparatus was built at University of Rennes in France (FALP-MS) [31,32]. In [32] the recombination coefficient of $\alpha = 1.5 \times 10^{-7}\,\mathrm{cm^3\,s^{-1}}$ for H_3^+ with a low degree of vibrational excitation $v < 2$ was found. In the same paper, the rate coefficient $\alpha = 1.1 \times 10^{-7}\,\mathrm{cm^3\,s^{-1}}$ for ground state ions $H_3^+(v = 0)$ at 650 K was reported. It started to be obvious that the rate of recombination depends on the vibrational state of the recombining ion. Therefore, in [31], the quenching rate of vibrationally excited H_3^+ ions in collisions with H_2 was also discussed. Canosa et al. in [32] proposed new model for recombination of H_3^+. In 1993, Smith and Španìl made precise measurements using the FALP and found the value $\alpha = (1\text{–}2) \times 10^{-8}\,\mathrm{cm^3\,s^{-1}}$ for $H_3^+(v = 0)$ at 300 K [33,34]. In 1995, Gougousi et al. [35] made a new FALP study of the recombination of H_3^+ ion. They suggested that H_3^+ recombination might proceed via three-body process that involves the formation of autoionising Rydberg states that are stabilised by collisions with H_2. The recombination rate coefficients obtained for H_3^+ and D_3^+ in previous studies known to us are given in Table 1 and Fig. 1. Recent observations of H_3^+ in both diffuse and dense interstellar clouds [36,37] raised new wave of studies of recombination of this ion at low temperatures.

Having experience with both SA and FALP, we assumed that the disagreement of the values for α_H and α_D in different experiments could be partly in the very low value of α ($\approx 10^{-8}\,\mathrm{cm^3\,s^{-1}}$). In majority of SA and FALP experiments, this value is closer to the lower limit of the used techniques; that were designed and usually applied for measurements of faster recombination rates (10^{-7} to $10^{-6}\,\mathrm{cm^3\,s^{-1}}$). The problem is also in the three-body character of the recombination process and very low number density of hydrogen at which process approaches the “high pressure limit” [38].

We are, however, not competent to comment results of beam studies (for discussion and references see, e.g., recent reviews by Schneider et al. [39] and by Tanabe et al. [40] and references therein). These techniques are very powerful, nevertheless they suffer two disadvantages: possibility of internal excitation of recombining ions and presence of strong electromagnetic field. For recent theoretical attempt of description of dissociative recombination of H_3^+ see, e.g., papers of Schneider et al. [41], Flannery [29], and very recent paper of Kokoouline et al. [42] and references therein.

Keeping in mind the advantages and limitations of the methods used in previous studies and trying to resolve the described problem, we recently built a new stationary afterglow experiment. In order to reduce the

Table 1
Selected experimental studies of the recombination of H_3^+ and D_3^+ ions with electrons

Number	α [10^{-7} cm^3 s^{-1}]	Method	Year	Comment	Authors	Reference
Recombination of H_3^+ ions						
1	25	SA/μw	1949		Biondi and Brown	[24]
2	20 and 60	SA/μw	1951	At 1 and 7 Torr of H_2	Richardson and Holt	[25]
3	3 and 25	SA/μw	1951	At 3 and 30 Torr of H_2	Varnerin	[26]
4	<0.3	SA/μw	1955		Persson and Brown	[27]
5	2.3	SA/μw	1973	300 K	Leu et al.	[46]
6	2.5	IB	1974		Peart and Dolder	[47]
7	2.1	MB	1977		Auerbach et al.	[48]
8	1.5	IT	1978		Mathur et al.	[49]
9	2.1	MB	1979		McGowan et al.	[50]
10	≤0.2	FALP	1984		Adams et al.	[28]
11	1.5	SA	1984		MacDonald et al.	[51]
12	≤0.0001	FALP	1987	Estimation	Adams and Smith	[52]
13	0.2	MB	1988	$v = 0$	Hus et al.	[53]
14	1.8	IR	1990	$v = 0$, very early afterglow	Amano	[30]
	1.5			$v \leq 2$		
15	1.1	FALP-MS	1991	$v = 0$	Canosa et al.	[31]
	1.5			300 K, $v \leq 2$		
16	1.1	FALP-MS	1992	650 K, $v = 0$	Canosa et al.	[32]
	1.5			300 K, $v \leq 2$		
17	0.1–0.2	FALP	1993	$v = 0$	Smith and Španìl	[33,34]
18	<2	IR	1994	$v = 0$	Feher et al.	[54]
19	1.15	SR	1994		Larson and co-workers	[55,56]
20	1.4–2	FALP	1995	0.01–0.1 Torr of H_2	Gougousi et al.	[35]
21	0.78	FALP-MS	1998		Laube et al.	[57]
22	0.7	SR	1999		Tanabe et al.	[40]
23	0.7	CRYRING	1999		Schneider et al.	[39]
24	<0.4	AISA	2000	$n(H_2) < 5 \times 10^{11}$ cm^{-3}, 2 Torr of He	Kudrna et al.	[58]
25	<0.13	AISA	2000	Dependent on [H_2], 2 Torr of He	Glosík et al.	[43]
26	1	ASTRID	2001		Jehnsen et al.	[59]
27	<0.04	AISA	2001	Dependent on [H_2], 2 Torr of He	Glosík et al.	[44]
Recombination of D_3^+ ions						
1	<0.2	FALP	1984	95 and 300 K	Adams et al.	[28]
2	0.8	FALP	1993	$v > 0$, 300 K	Smith and Španìl	[33]
	0.2			$v = 0$		
3	0.75–1.4	FALP	1995	Dependent on [D_2]	Gougousi et al.	[35]
4	0.27	CRYRING	1997		Larsson et al.	[60]
5	0.27	CRYRING	1998		Le et al.	[61]
6	0.67	FALP-MS	1998	0.5 Torr of He, 300 K	Laube et al.	[57]
7	<0.06	AISA	2002	Dependent on [D_2], 2 Torr of He	Poterya et al.	[45]

The cross sections obtained in some studies were recalculated to rate coefficients. Methods: SA: stationary afterglow (μw—microwave measurement of electron density), IB: inclined beam, IT: ion trap, FALP: flowing afterglow with Langmuir probe, AISA: advanced integrated stationary afterglow, IR: infrared stationary afterglow-absorption spectroscopy, SR: storage ring, MB: merged beam.

diffusion losses and hence to prolong the duration of decay of the plasma to tens of milliseconds we used comparatively large discharge vessel. With the intention to well define the conditions of the experiment, we made the vacuum vessel and gas handling systems using UHV technology. The used gases were also additionally purified. Moreover, we kept the impurities at lowest level by flowing comparatively large flow of pure He through the discharge chamber during the experiment.

In this review, we give more extended description of instrument, used diagnostics and tests. We will

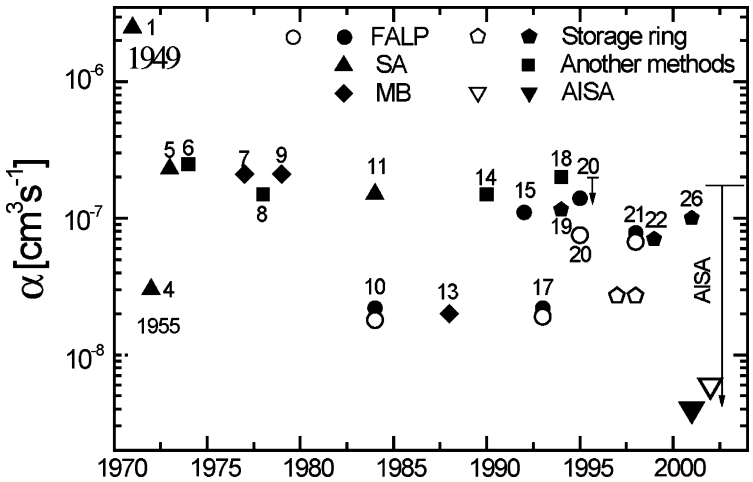

Fig. 1. Experimental rate constants of recombination of H_3^+ (closed symbols) and D_3^+ (open symbols). Numbers indicate number in Table 1 where references are given.

report here the results of our studies of the recombination of H_3^+ and D_3^+ ions with electrons [43–45]. We have also presented further experimental results relevant to independence of α on He pressure and further measurements towards higher $[H_2]$ and $[D_2]$. In the present study, we also carefully examine various features of the method and of the instrument in order to gain confidence in the obtained experimental results. Particular attention is paid to ionic composition during plasma decay and its determination by computing and measurements of the time resolved mass spectra. We also discuss possible influence of internal excitation of recombining ions.

2. Experiment

The main part of the AISA instrument is the cylindrical stainless-steel discharge chamber—see Fig. 2. The UHV main chamber, made by Vakuum Praha, was 40 cm in diameter and 40 cm in length. The chamber is pumped by turbomolecular pump. The ultimate background pressure reached after the bake-out at 140 °C from 2 days was less than 5×10^{-9} Torr. The vacuum chamber is equipped by a series of entry-ports sealed by the standard Con-Flat flanges. The largest port is positioned at the vessel axis and has a diameter of 180 mm. This port holds a quartz window for passing the microwave power into the chamber. On the opposite side of the vessel there is a smaller flange 100 mm in diameter that carries the quadrupole mass spectrometer instrument by HIDEN. The mass spectrometer chamber is differentially pumped by turbomolecular pump. The ultimate background pressure in the mass spectrometer/plasma monitor chamber reached after the bake-out up to 100 °C is $<1 \times 10^{-9}$ Torr. The discharge chamber and the differentially pumped quadrupole chamber are separated by the electrically insulated molybdenum foil with an orifice diameter 0.1 mm used for sampling ions into the input ion optics of the mass spectrometer. From the same side as the quadrupole sticks into the discharge chamber the cylindrical Langmuir probe with its collecting surface placed 6 cm in front of the sampling orifice and just 2.5 cm out of the axis of the discharge chamber, see Fig. 2. The gas entry ports are mounted on a single flange so that there is good mixing of gases prior to entering the chamber. On the top of the chamber there is a small observation window. A photodiode fixed to the large window is used to monitor the stability and reproducibility of the discharge.

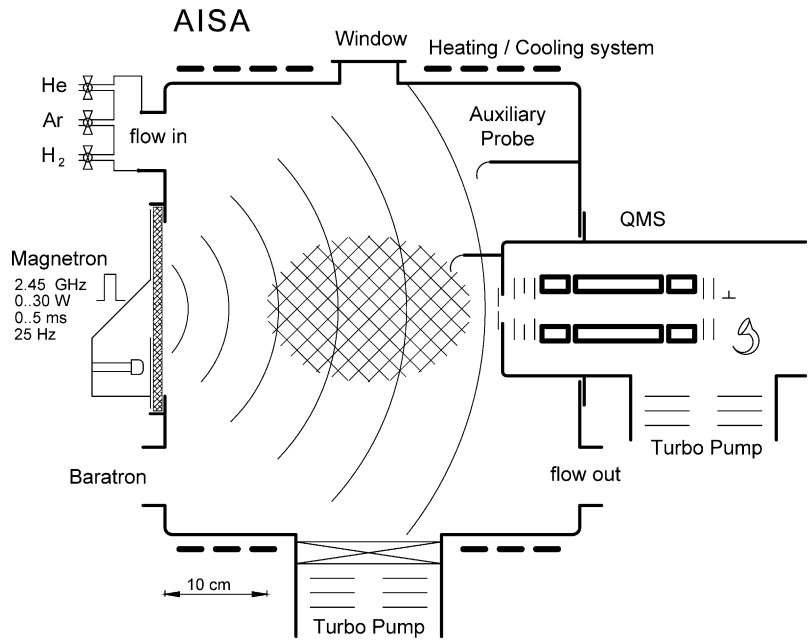

Fig. 2. Schematic view of the advanced integrated stationary afterglow (AISA) instrument. The microwaves generated by magnetron enter the discharge chamber via large quartz window.

The gas pressure in the discharge chamber (1.5–3 Torr) is measured by MKS Baratron capacitance manometer. The mass-flows of the buffer and reactant gases are measured and controlled by three MKS mass-flow-controllers.

Even if the residual pressure reached in the discharge chamber is at very low level there is a constant flow of impurities desorbing of the chamber walls, partly enhanced by the discharge. This effect may deteriorate the purity of the gas filling during the measurements. To prevent this, the flow of impurities is diluted by comparatively large flow of very pure He, up to 1000 sccm, flowing through discharge vessel under action of large roots pump. Using this large flow the buffer gas in the discharge volume is replaced within 10 s. In this sense, the AISA utilises advantages of both the stationary and the flowing afterglow techniques. In our experiment, we used He grade 5.0 as the buffer gas. He was additionally purified by passing through two liquid nitrogen traps filled with zeolite. Also the discharge chamber was cooled below $-30\,^{\circ}C$ during the measurements to suppress the residual pressure of water. High purity of the vacuum system and fast pumping minimises the possibility of negative ion formation.

The estimation of the optimum flow of buffer and reactant gas required some consideration. The flow velocity of He buffer gas in classical FALP [28] or its modification FALP-MS [31] or HPFA [62,63] is comparatively high, of the order 50–100 ms^{-1}. With 0.5 m long reaction/recombination region, the afterglow plasma can hence be observed for 5–10 ms. Within these 10 ms, the reactive losses have to be negligible in comparison with losses due to recombination. In the present AISA instrument, we can measure up to 100 ms; therefore, level of impurities that cause reactive losses, has to be 10 times lower. By considering residual pressure, pumping speed of turbo pumps, flows of He, Ar and H_2 (or D_2) used in experiments, we estimated that there is less as 0.2 ppm of unwanted impurities in the buffer gas in the discharge vessel. The mass spectra obtained by the sampling of ions from the discharge and the decay of the plasma confirms this estimation (see Section 8).

Pulses of microwave power ignite the discharge. Magnetron tube with nominal power exceeding 1 kW is used for this purpose. The mains transformer with high-voltage secondary winding followed by a half-wave rectifier create the anode voltage of the magnetron (approximately 6 kV). The anode voltage is switched on and off by a high-tension switch HTS81 (BEHLKE electronic GmbH) in synchronism with the mains frequency so that only during the part of the voltage half-wave the magnetron generates the microwave power. This arrangement gives the possibility to vary the microwave power consumed in the discharge by varying the pulse width (0.2–5 ms was used). The variation of the discharge repetition period is also possible (must be the multiple of 20 ms) in the range from 20 to 100 ms.

In order to achieve good accuracy of the measured α the observed dynamic range of the electron density decay has to be over one order of magnitude. This requests in the experiment comparatively long time of observation and high initial plasma density. For instance, in order to achieve the plasma density decay of 30 ms in duration, we need to have the initial plasma density $n_{e0} = n_e(t = 0) \approx 10^{10}\,\mathrm{cm}^{-3}$ or higher (calculated on the basis of Eq. (2)). Such initial plasma density can be achieved with used plasma generator (2.45 GHz, 1 kW). Positions of the probes, however, have to be suitably chosen in order to minimise the possible interference with standing microwave pattern inside the vacuum vessel during the active discharge phase.

Two electrostatic Langmuir probes were used in present experiment. In some measurements, the cylindrical platinum probe 7 mm long and 100 μm in diameter was used. In most of measurements, smaller tungsten probe 7 mm long with diameter 18 μm was used. The use of such thin probe reduces the drain of charged particles from the afterglow plasma [64] and also has been thoroughly examined for measurements of low electron temperatures [65]. Both probes were calibrated by procedure, which will be described below. We did not observe difference in obtained α when using different probes.

The electron number densities and their time evolutions were obtained from the probe characteristics. Actually in the experiment the current to the probe (I_P) was measured as a function of decay time (t) at constant probe potential (V_P). The probe potential was measured against the potential of the discharge vessel, which was grounded. The probe potential was changed by a constant value (voltage step) after every synchronisation pulse, in such a way that probe current was obtained as function (set of data $\sim 300 \times 500$) of time and probe potential, $I_P = I_P(t, V_P)$. The matrix could be re-measured several times and matrix of average values then constructed. From this function of two variables, the probe characteristics at given afterglow time t, $I_{Pt} = I_{Pt}(V_P)$, could be extracted. Similar method was used in [66,67]. The electron density at given t, $n_e(t)$, was obtained from the part of the probe characteristic corresponding to the probe electron current in the acceleration regime, namely from the slope of the I_P^2 vs. V_P plot (for more details see, e.g. [68–70]) and also from the electron probe current at plasma potential. From the second derivatives of the probe characteristics the electron energy distribution functions (EEDFs) and electron temperature (T_e) were calculated [68] and from its zero-cross the plasma potential estimated. Electron temperature T_e was also evaluated directly from the probe characteristic. We estimated from the probe data that for afterglow times later than approximately $t = 5$ ms the temperature of the electron gas equals roughly to the gas temperature, $T_e \approx 260 \pm 30$ K.

In Fig. 3, there is 3-D plot of $I_P = I_P(t, V_P)$ obtained in decaying plasma in pure He. As it will be explained below the time evolution (decay) is given just by ambipolar diffusion of He_2^+ ions and electrons, because the recombination of He_2^+ can be neglected in the used time scale [71]. Fig. 3 also demonstrates the quality of the experimental data.

In pulsed discharge in pure He, He^+ ions and the metastable atoms He(2^1S) and He(2^3S) are produced. More energetic He(2^1S) are rapidly converted [72] in super-elastic collisions with electrons to He(2^3S). The relatively long lived He(2^3S) metastables represent an additional source of ionisation in the early afterglow,

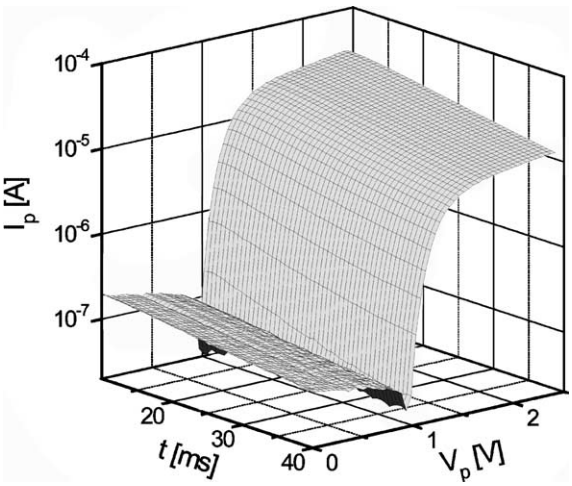

Fig. 3. Temporal evolution of the probe characteristics. 3-D plot of $I_P = I_P(t, V_P)$, in afterglow plasma with dominance of He_2^+ ions in pure He.

where they form He_2^+ ions in a very fast Penning ionisation (see, e.g., discussion and references in [71,73]). It is probable, that He_2^+ ions formed in this manner are electronically excited, but we assume that they are efficiently quenched in collisions with He (this is, however, not critical assumption in present study). Also, at the pressure 1.3–3.0 Torr, He^+ ions formed in discharge are converted in three-body association to He_2^+ in the early afterglow period. The pressure over 1.3 Torr is therefore, necessary to complete the conversion of He^+ into He_2^+ in the early afterglow period. HeH^+ ions are not formed in significant amount, not even traces of this ion were observed in mass spectra. Anyway if there will be HeH^+ produced during the active discharge or in early afterglow they will be immediately converted to ArH^+ by fast proton transfer and these ions are considered in our analysis. The examples of measured evolutions of the electron number density, $n_e(t)$, in He_2^+ dominated afterglow is plotted in Fig. 4. Note the small increase of n_e at $t <$ 10 ms due to the above-mentioned Penning ionisation process. For later afterglow times, the plasma decays by ambipolar diffusion since ground state He_2^+ ions recombine very slowly [71]. The dotted straight line indicates the calculated relative diffusion losses of He_2^+. The measured decay is a little faster indicating possibly small influence of the mass spectrometer sampling port and probably some limited presence of reactive losses also (see discussion of balance equations). The decay due to non-recombinative losses give us the lower limit for α measurable in present

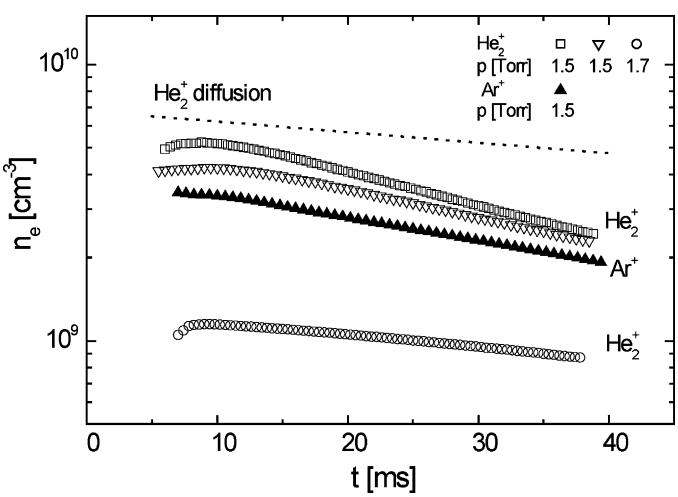

Fig. 4. Decays of He_2^+ and Ar^+ dominated "very slowly recombining" plasmas, $n_e(\tau)$. Corresponding He pressures are indicated. Note that curves, corresponding to He_2^+, obtained at lower and higher n_{e0} are parallel. The dotted straight line indicates the calculated losses purely due to ambipolar diffusion.

experiment. The limit is below 3×10^{-9} cm^3 s^{-1}. We use this comparatively easy measurable dependence as an indicator of the cleanliness of our discharge chamber. If the chamber were not clean enough than the decay of He_2^+ ions would be faster because of reactive losses. In such case, the experiment would have to be interrupted and the vacuum system additionally cleaned. At pressures used in our experiment (1.3–3 Torr), the reduction of the electron current due to elastic scattering of electrons by neutrals cannot be neglected. Even if the attempts have been done to estimate the magnitude of this effect [74,75], the results given in [74] have not been experimentally verified. Since for the estimation of the recombination rate coefficient, the precise absolute values of the electron density were necessary, the literature value of the recombination rate coefficient of recombination of O_2^+ ions with electrons [69,76,77] has been used for determining the "calibration factor" which accounts for used pressure of He. O_2^+ ions were produced by adding ∼0.5 sccm of O_2 to He. The low partial pressure of O_2 could not influence the collection efficiency of the Langmuir probe (by creating tungsten oxides on the probe surface). The obtained decay of n_e is plotted in the upper panel of Fig. 5, the reciprocal data $1/n_e$ are plotted in the lower panel of Fig. 5. From the slope of the linear fit to the part of the $1/n_e$ plot corresponding to the time interval where the plasma decay is controlled predominantly by recombination, the α can be calculated. Small deviation of the $1/n_e$ plot from linearity at higher t is supposedly due to diffusion. In exact calculation, α is determined as a parameter of the fit to the data when the diffusion losses are also considered—see discussion. These fits are also depicted in Fig. 5. In the present experiment, the calibration was made at the pressure 2.3 Torr. By the process of calibration, we estimated the "calibration factor" that corresponded to the effect of the electron current decrease due to the effect of electron–neutral collisions. Its value estimated by the calibration procedure described above was 1.4 ± 0.2 for the 18 μm diameter probe, and it corresponded roughly to the factor describing the reduction of the electron current due to electron–neutral collisions in theory [74]. In all values of n_e plotted in Fig. 5 and in the following figures this calibration is already considered.

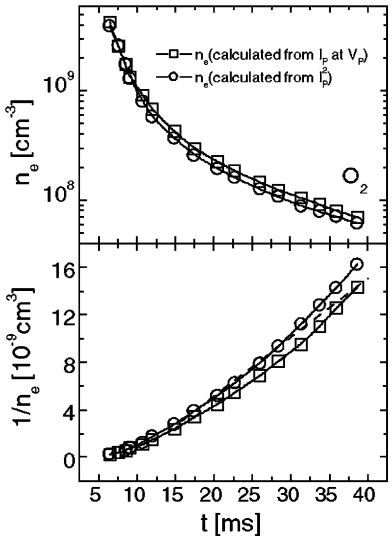

Fig. 5. Upper panel: temporal evolution of the electron number density, $n_e(t)$, in the O_2^+ dominated plasma. The values of $n_e(t)$ obtained from "I_P^2 vs. V_P plots" are plotted by circles. The values obtained from the probe currents at plasma potential are plotted by squares. The lines indicate best fit of the data by Eq. (2). Lower panel: $1/n_e$ vs. decay time t. The values of $n_e(t)$ are obtained by two methods. The lines represent best fit of the data by Eq. (2). Dashed straight line indicates fit of the data in recombination-dominated interval.

3. The evaluation of the recombination rate coefficient from the decay of electron density

We will demonstrate our method of evaluation of recombination rate coefficients from measured decay of the electron number density on the data obtained for O_2^+ dissociative recombination. It is partly because value of $\alpha_{DR}(O_2^+)$ is well known and partly because formation of O_2^+ dominated afterglow is easy, fast and not very sensitive to impurities. Despite the fact that we do not have problems with impurities we include in our analyses also possibility that some ions are converted to "impurity ions" which immediately recombine. If O_2^+ ions are dominant ions and they are removed from plasma only due to the processes

of recombination, ambipolar diffusion and reactions, which are characterised by α, ν_D (see, e.g. [78]) and ν_R, respectively, the balance equation for electrons can be in first approximation written as

$$\frac{dn_e}{dt} = -\alpha[O_2^+]n_e - \nu_D n_e - \nu_R n_e = -\alpha n_e^2 - \nu_D n_e - \nu_R n_e \quad (1)$$

We assume neutrality of the plasma, $[O_2^+] = n_e$. For negligible diffusion and reactive losses ($\nu_D = \nu_R = 0$) the solution of the equation is $1/n_e = 1/n_{e0} + \alpha t$. If also diffusion is considered and the reactive losses were negligible ($\nu_R = 0$), the solution could be written in the form:

$$\frac{1}{n_e} = \frac{\exp(\nu_D t)}{n_{e0}} + \alpha\frac{\exp(\nu_D t) - 1}{\nu_D} \quad (2)$$

Here n_{e0} is the electron number density at $t = 0$ [77]. In the following analysis, however, we shall treat the general case ($\nu_D \neq 0$, $\nu_R \neq 0$). The diffusion losses generally depend on the geometry of the discharge chamber, on pressure and on the electron and the buffer gas temperatures. The parameter ν_D can be calculated and/or obtained from experimental data. Eq. (2) is used to fit data in Fig. 5. Because of the high quality data, dn_e/dt can be calculated and the balance Eq. (1) can be rewritten to the form suitable for evaluation of α (using n_e' for dn_e/dt):

$$\frac{-n_e'}{n_e^2} = \alpha + \frac{(\nu_D + \nu_R)}{n_e} \quad (3)$$

The value ν_D was obtained experimentally from decay of He_2^+ and Ar^+ dominated afterglow and confirmed by calculation from geometry of the discharge chamber, see Fig. 4. When ν_D is known, the values $(-n_e'/n_e^2 - \nu_D/n_e)$ can be plotted vs. $1/n_e$. The obtained dependence should be linear, the slope of the plot gives value ν_R and zero intersection gives the value α. Example of such plot for O_2^+ dominated afterglow is given in Fig. 6. Note that because the recombination of O_2^+ was used for the calibration the obtained rate of recombination must be equal to the literature value, i.e., $\alpha = 2 \times 10^{-7}\,cm^3\,s^{-1}$. Fast slope at early afterglow times corresponds to the formation of O_2^+ dominated plasma. Advantage of this "advanced analysis"

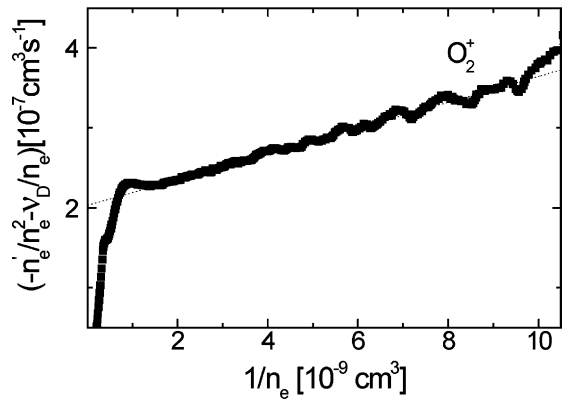

Fig. 6. Advanced analysis—dependence of $(-n_e'/n_e^2 - \nu_D/n_e)$ vs. $1/n_e$, corresponding to the decay of O_2^+ dominated plasma.

is in that determination of α is independent of diffusion and reactive losses, as long as corresponding terms in balance equation are linear, i.e., in the (acceptable) approximation of first diffusion mode and small reactive losses. Computer simulations of the plasma decay for several initial distributions verified the validity of the approximation of the first mode diffusion. The validity of the approximation is also supported by measurements of the decays of He_2^+ and Ar^+ dominated afterglow; see Fig. 4.

In case of H_3^+ dominated afterglow the balance equation for electrons can be in first approximation written in a pattern similar to (1):

$$\frac{dn_e}{dt} = -\alpha[H_3^+]n_e - \nu_D n_e - \nu_R n_e = -\alpha f n_e^2 - \nu_D n_e - \nu_R n_e \quad (4)$$

Here we shall pursue the analysis of the balance equation for H_3^+ in H_2 containing plasma, but the procedure would be analogous for D_3^+ in deuterium containing plasma. We take into account also the presence of other ions in the decaying plasma by the following consideration: we assume that in formed plasma there is fraction $f = f(t) = [H_3^+]/n_e$ of recombining H_3^+ ions and that the other ions are "not recombining" (predominantly Ar^+, ArH^+, He_2^+). If the plasma were governed solely by recombination of H_3^+ then the solution of this equation would read

$1/n_e = 1/n_{e0} + \alpha f t$. This formula is usually used to obtain α from the slope of the plot of $1/n_e$ vs. t, under assumption $f = 1$. Because of the high quality data, $n'_e = dn_e/dt$ can be calculated and the balance Eq. (4) can be rewritten as

$$\frac{-n'_e}{n_e^2} = \alpha f + \frac{(\nu_D + \nu_R)}{n_e} = \alpha_{eff} + \frac{(\nu_D + \nu_R)}{n_e} \quad (5)$$

The fraction $f(t)$ can be estimated from calculation of ionic composition and/or from mass spectrometric data. For $[H_2] > 10^{11}\,cm^{-3}$, H_3^+ ions are formed within $t \sim 10$ ms (see discussion) and $f \sim 1$ can be used to obtain α. The plot of $-n'_e/n_e^2$ vs. $1/n_e$ should be linear with slope given by $(\nu_D + \nu_R)$. Because of high purity of the vacuum chamber, the term $\nu_R n_e$ represents just small correction. For low $[H_2] < 10^{11}\,cm^{-3}$, the formation of H_3^+ is slow and $f < 1$ at low t. However, as the data are good enough we can calculate in such case $(\nu_D + \nu_R)/n_e$ from the "late afterglow" and by plotting $(-n'_e/n_e^2 - (\nu_D + \nu_R))$ vs. $1/n_e$, the evolution of αf can be obtained. This can be useful, e.g., if during decay of plasma α is constant and a fraction is dependent on decay time. In the last part of Eq. (5), we introduced effective rate coefficient, $\alpha_{eff} = \alpha f$. It is good to use α_{eff} if we cannot simply separate $\alpha(t)$ and $f(t)$. If $f(t) = 1$ than $\alpha_{eff} = \alpha$, this is situation for $[H_2]$, $[D_2] > 2 \times 10^{11}\,cm^{-3}$. To avoid introduction of some sort of assumptions we will use α_{eff} as pure experimental quantity to describe obtained experimental results. Only at the end we will use mass resolved spectra and kinetic model to comment the results. Because of large scale of values of obtained α by all three methods, approximations were used and results were compared to obtain best value of α.

4. The probe measurements

The decay of the afterglow plasma is very slow at present experimental conditions, the characteristic time of the decay of n_e is of the order of many milliseconds. During the decay time, the electrons undergo multiple elastic collisions with He atoms and hence they are thermalised to buffer gas temperature. It was estimated in [79] that in He, at the pressure over 1 Torr, the electron temperature relaxation time in He afterglow plasma is of the order of several microseconds. To have the confidence, that the afterglow plasma is in thermodynamic equilibrium, and that the measured electron temperature, T_e, really corresponds to Maxwellian distribution of electron energies, the electron distribution function was measured. For this measurement, the Druyvesteyn method [80] and Šícha et al. [81] has been applied. Because of the high quality of the measured probe data it was possible to calculate numerically (using the Savitzky–Golay [82] approach) the second derivatives of the probe current with respect to the probe voltage (I''_P) and consequently the EEDF. The good linearity of I''_P in the semilogarithmic plot vs. the probe voltage indicates that the experimentally estimated EEDF is very close to Maxwellian. We calculated the electron temperature as a function of the afterglow time, $T_e(t)$, by the "classical" method from the slope of the linear part of the semilogarithmic plot of the electron probe current I_P vs. the probe voltage in the electron retarding range of probe voltages. We also checked that the electron temperature determined in this manner corresponded within the estimated experimental errors to that determined in similar manner from the plot of $\log(I''_P)$ vs. the probe voltage. In Fig. 7 example of the measured dependence $T_e(t)$, obtained in Ar^+ dominated afterglow is plotted. Data obtained by both methods, together with estimated experimental errors are plotted. It is seen from Fig. 7 that beginning at afterglow time ~5 ms, the T_e relaxed almost down to the buffer gas temperature. The relaxed T_e found experimentally is by 10–30% higher than the gas temperature. That is systematic error. In the actual experiment fluctuations of probe and plasma potential, changes of the work function and plasma potential over the probe surface influence (distort) the measured probe characteristic. Consequently, the apparent electron temperature estimated from such probe data may be slightly higher (we talk about difference approximately 100 K, i.e., 10 meV in energies) than in reality. Taking this effect into account, we conclude that for afterglow times later than approximately

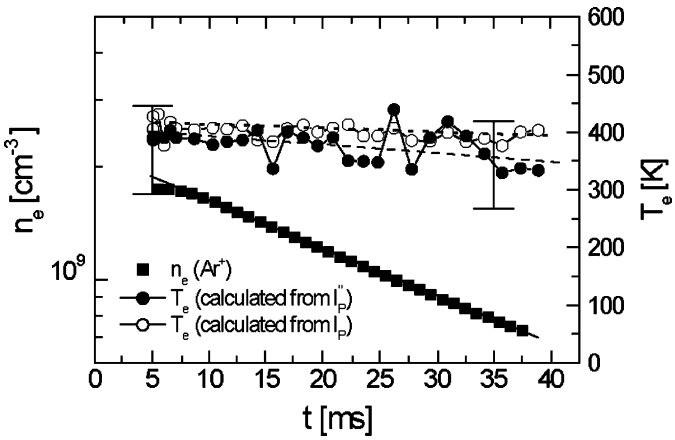

Fig. 7. Time evolution of electron temperature, $T_e(t)$, in Ar^+ dominated afterglow in He–Ar mixture ($p_{He} = 2$ Torr). Solid circles—values evaluated from the second derivatives of the electron parts of the probe characteristics, I_p''. Open circles—values deduced from I_P. Solid squares—measured corresponding evolution of electron density $n_e(t)$.

$t = 5$ ms, the temperature of the electron gas equals to the gas temperature, $T_e \approx 260 \pm 30$ K $\approx T_g$. This fact suggests that (i) the processes that contribute to the electron gas heating during the afterglow period may be considered to have a negligible effect and (ii) the quality of the probe data and the method of its evaluation enables estimation of such low electron temperatures. The credibility of the probe technique supports also the application of the extremely thin probe with the diameter of 18 μm. The use of such thin probe reduces the drain of charged particles from the afterglow plasma [64] and also has been thoroughly examined for measurements of low electron temperatures [65]. The consequent comparatively high Knudsen number $K_e = \lambda_e/r_p$ minimises also the effect of collisions of electrons with neutrals in the space charge sheath around the probe on the probe data (λ_e and r_p is electron-free path and probe radius, respectively). Such a thin probe is therefore, applicable at elevated pressures (several Torr) at which our measurements have been made [74,83]. Also in H_3^+ and D_3^+ dominated afterglow we observed $T_e \approx T_g$ and we are therefore, convinced that we measure the correct rate of H_3^+ recombination in truly thermalised plasma.

5. The formation of H_3^+ and D_3^+ ions

The main goal of the present study was the recombination of H_3^+ and D_3^+ ions. Again we will write about formation of H_3^+ in He:Ar:H_2 having in mind that in similar way D_3^+ ions are formed in He:Ar:D_2. That is because in considered ion–molecule reactions hydrogen and deuterium molecules react with comparable rate coefficients.

In order to study this recombination, we have to produce plasma with dominant population of H_3^+ ions. In present experiment, this cannot be simply achieved by having discharge in pure hydrogen or in mixture of H_2 with He buffer. To convert all ions formed in the active discharge to H_3^+ ions it is necessary to add 0.1–1% Ar and traces of H_2 to He buffer and to form at first Ar^+ ions which further react to produce H_3^+. This conversion proceeds in the very early afterglow period. If we assume that during microwave pulse, the electrons have temperature of several eV, then ionisation frequency for ionisation of Ar is comparable with ionisation frequency for ionisation of He even if in the mixture there is only 0.2% Ar [84]. This is because of higher cross section for ionisation of Ar and high ionisation potential of He. In Fig. 8, the integral

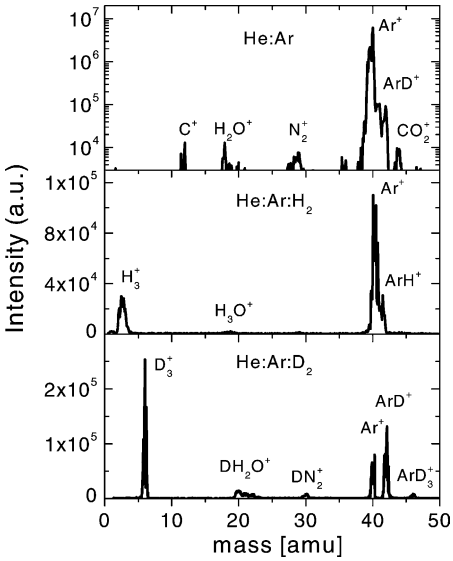

Fig. 8. Examples of integral mass spectra obtained in He:Ar, He:Ar:H_2 and He:Ar:D_2 mixtures are plotted in upper, middle and lower panel, respectively.

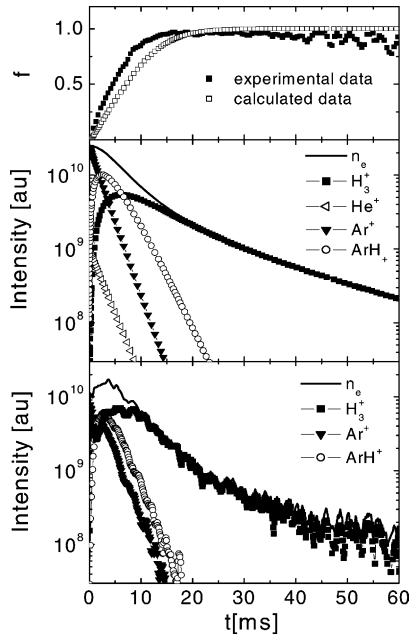

Fig. 9. In the lower and middle panel there is plotted measured and calculated time evolution of ionic composition ($[H_2] = 2.7\times10^{11}$), respectively. The time resolved mass spectrum giving relative ionic population is normalised in the plot to $n_{e0} = 2.5 \times 10^{10}\,cm^{-3}$ in agreement with data obtained by the Langmuir probe. The calculation was made for conditions corresponding to experiment, under assumption that $n_{e0} = 2.5 \times 10^{10}\,cm^{-3}$ and that there is 90% of Ar^+ and 10% of He^+ ions at the beginning of the decay. In the upper panel the "f" functions obtained from experiment and from the kinetic model are plotted.

mass spectra, i.e., the spectra obtained by integration of the respective ion signal during both the active discharge and the afterglow periods are plotted. In the upper panel there is spectrum obtained in He–Ar mixture with only residual presence of D_2 from previous experiments (source of ArD^+). Note the very low level of ions from impurities (mainly H_2O, N_2). Low resolution in mass spectrometer was used deliberately to increase its sensitivity. In the medium and lower panels there are spectra obtained when traces of H_2 and D_2 were added to the He–Ar mixture. In the mass spectra, we did not observe He^+ and $He_2{}^+$. To observe these ions, it was necessary to reduce the partial pressure of Ar substantially. Partly it is because the mass spectrometer sampling orifice is close to the chamber wall and it takes many milliseconds for ions formed in the chamber volume to reach this place. During this time, majority of He^+ and $He_2{}^+$ ions are converted in ion–molecule reactions to Ar^+, ArH^+ and finally to $H_3{}^+$. Partly it is also because of efficient ionisation of Ar in comparison with He, as it was already mentioned. For better understanding of processes of formation and their time dependences we measured "time resolved spectra"—the time evolutions of the relative population of the ions. These spectra were made for ions identified in integral mass spectra. In the lower panel of Fig. 9 measured evolutions of relative number densities of Ar^+, ArH^+ and $H_3{}^+$ are plotted.

The mass spectrometer gives important but not sufficient information about an ionic composition in recombining plasma. To gain further information and to confirm mass spectrometer and probe data, we constructed the kinetic model of the decaying afterglow plasma. Calculation was made by solution of the set of balance equations and also by Monte-Carlo simulation. The calculations were done for many sets of initial conditions because it is difficult to evaluate composition of the plasma after short microwave pulse. As it was already mentioned comparison of the

ionisation frequencies for Ar and He, for used mixtures, gives comparable rate of formation of Ar^+ and He^+. It is crucial to use He pressure over 1.3 Torr and higher to enhance three-body association in which He^+ and eventually H^+ are converted to molecular ions. Basically, if He^+ are formed they are converted to $He_2{}^+$ and the chain of reactions proceeds by reaction with Ar and formation of Ar^+. Just formed Ar^+ reacts further in fast binary reaction with H_2 and ArH^+ (major channel) or $H_2{}^+$ (minor channel) are formed [85]. The last step in the sequence is the formation of $H_3{}^+$ ions by proton transfer reaction from both ArH^+ and $H_2{}^+$ to the neutral H_2 [19]. Metastable $He(2^3S)$ atoms that are possibly formed in the discharge react fast also with Ar atoms and Ar^+ ions are produced [69]. In Table 2 reactions are listed, which take place in sequence of reactions resulting in $H_3{}^+$ dominated afterglow. In Table 2 there are also given reaction rates and characteristic time constants at the reactant number densities typical for present experiments.

Note, that at all used partial pressures of He, Ar and H_2, the reaction times were shorter than 7 ms. It follows that the overall time constant of $H_3{}^+$ ions formation is less than 10 ms and the time necessary for conversion of ~90% of all the ions into $H_3{}^+$ ions is less than 20 ms. Exact time evolution of the ionic composition for the used mixtures of the gases was calculated. Examples of obtained evolutions are plotted in middle panel of Fig. 9. In the calculation, it was assumed that in the active discharge was formed 90% of Ar^+ and 10% of He^+. He^M are not considered, because they are immediately converted by Penning ionisation to Ar^+. Diffusion and recombination processes of the respective ions were also taken into account. Fraction $f(t)$ obtained from measured and calculated evolutions are plotted in the upper panel of Fig. 9. In Fig. 10 calculated and measured time resolved spectra together with integral spectra obtained by measurements and by integration of time resolved spectra are plotted. Very good consistency of data is noted. All the calculations confirmed the estimation given in Table 2. Only at very low hydrogen number densities, $[H_2]$, approaching $1 \times 10^{11}\,cm^{-3}$ the time necessary for conversion of most ions into $H_3{}^+$ was longer than 15 ms. For $[H_2] < 1 \times 10^{11}\,cm^{-3}$ the formation of $H_3{}^+$ ions have to be considered when evaluating recombination rate coefficient. Factor "f" was calculated and measured for these low number densities and "advance analysis" was used to determine recombination rate coefficients. In the lower panel of

Table 2
Reactions, those take place in the formation of $H_3{}^+$ ions

Reaction number	Reaction	Rate coefficient [$cm^3\,s^{-1}$] or [$cm^6\,s^{-1}$]	Reactant number density [cm^{-3}]	Reaction time [ms]	Reference
1	$He^+ + 2He \rightarrow He_2{}^+ + He$	1×10^{-31}	6.5×10^{16}	2	[17]
2	$He^M + He^M \rightarrow He_2{}^+ + e$	5×10^{-9}	5×10^{10} (assumption)	4	[73]
3	$He^M + Ar \rightarrow Ar^+ + He + e$	7×10^{-11}	1×10^{14}	0.14	[69]
4	$He_2{}^+ + Ar \rightarrow Ar^+ + 2He$	2×10^{-10}	1×10^{14}	0.05	[17]
5	$Ar^+ + H_2 \rightarrow ArH^+ + H$ $\rightarrow H_2{}^+ + Ar$	8×10^{-10}, ArH^+ production is dominant	2×10^{11}	6.3	[85]
6	$H_2{}^+ + Ar \rightarrow ArH^+ + H$	2.3×10^{-9}	1×10^{14}	<0.01	[19]
7	$H_2{}^+ + H_2 \rightarrow H_3{}^+ + H$	2.1×10^{-9}	2×10^{11}	2.4	[19]
8	$ArH^+ + H_2 \rightarrow H_3{}^+ + Ar$	1.5×10^{-9}	2×10^{11}	3.3	[86]
9	$H_3{}^+ + H_2 + He \rightarrow H_5{}^+ + He$	$<1 \times 10^{-29}$	2×10^{11}, 6.5×10^{16}	>8000	[20]
10	$H_3{}^+ + H_2 + H_2 \rightarrow H_5{}^+ + H_2$	4.6×10^{-30}, 210 K	2×10^{11}	$>1 \times 10^9$	[22]
11	$H^+ + He + He \rightarrow HHe^+ + He$	0.9×10^{-31}	6.5×10^{16}	2.6	[87]

He^M indicates $He(2^3S)$. The rate coefficients of binary reactions are given in $cm^3\,s^{-1}$, the rate coefficients of the three-body association are given in $cm^6\,s^{-1}$. The rate coefficients for the reactions of $H_2{}^+$ are given for ions with vibrational excitation $v \leq 1$. The time constants—reaction time are calculated for $[He] = 6.5 \times 10^{16}\,cm^{-3}$ and $[H_2] = 2 \times 10^{11}\,cm^{-3}$.

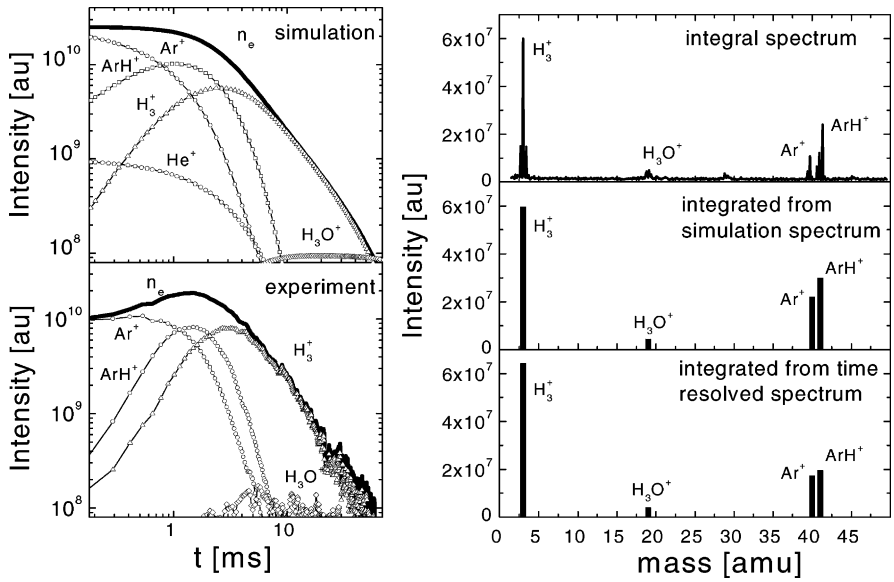

Fig. 10. The calculated and measured time evolutions of the ionic composition during the afterglow in He:Ar:H_2 plasma ($[H_2] = 6.7 \times 10^{11}$). The time resolved (experimental) mass spectra, which are measured in arbitrary units, are normalised to initial $n_{e0} = 2 \times 10^{10}\,cm^{-3}$ in agreement with value obtained by Langmuir probe. The same number density was used as the initial condition in calculation. The corresponding measured integral spectra are plotted in the right panels.

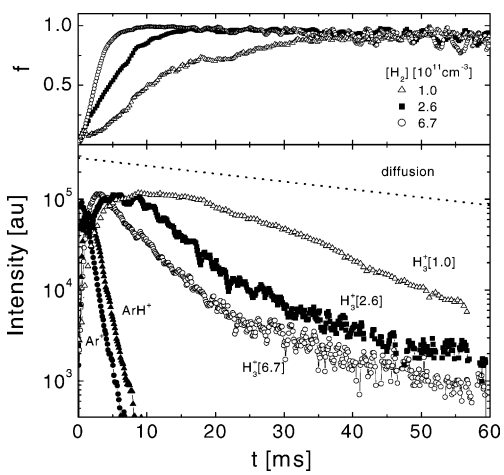

Fig. 11. Lower panel: the time resolved mass spectra obtained at several different concentration of H_2. For $[H_2] = 6.7 \times 10^{11}\,cm^{-3}$ the corresponding decays of Ar^+ and ArH^+ are also plotted. The rates of the corresponding ion–molecule reactions obtained from the decays agree (within the accuracy of the experiment) with values written in Table 2. The dashed straight line indicates pure diffusive losses. Upper panel: the plots of corresponding evolutions of the fraction *f*.

Fig. 11 several time resolved spectra for H_3^+ ions obtained at several number densities of hydrogen are plotted and the corresponding *f* factors are plotted in the upper panel.

We did not consider up to now the internal excitation of the reacting ions. We assumed that after 10–15 ms of "formation time" the possible internal excitation of H_3^+ is quenched in multiple collisions with He, Ar and H_2 (see, e.g., discussion and estimation of the quenching rate coefficient by Smith and Španìl in [33]). The discussion of internal excitation of H_3^+ is important for some experiments, because it is expected that excited states of this ion recombine faster than the ground state.

6. Possibility of vibrational excitation of recombining ions

The influence of vibrational excitation of H_3^+ and D_3^+ ions on the rate of their recombination was discussed many times [30–34,54,57] as the possible reason for differences in experimental results. In

some experiments, the recombination rate coefficient was determined explicitly for $H_3^+(v = 0)$. We have made simple calculation of a decay of the plasma under assumption that at the beginning of the decay it contains two types of ions, $H_3^+(v = 0)$ and $H_3^+(v > 0)$ with different recombination rate coefficients. We will show below that the recombination coefficients of H_3^+ and D_3^+ ions can be smaller as $10^{-8}\,cm^3\,s^{-1}$. That is why we assumed in this calculation that $\alpha_1 = \alpha_1(v = 0) = 1 \times 10^{-8}\,cm^3\,s^{-1}$ and $\alpha_2 = \alpha_2(v > 0) = 2 \times 10^{-7}\,cm^3\,s^{-1}$. In the upper panel of Fig. 12, obtained changes in relative populations of both types of ions during the afterglow for several initial conditions are plotted. Note that fast recombining ions are very efficiently removed from the plasma within 10 ms even if their initial population is very high. In the lower panel, corresponding decay curves are plotted, it is evident at $t > 10$ ms influence of fast recombining ions can be neglected. We can conclude, that "by skipping" 10–15 ms of the early decay we can neglect the influence of vibrational excitation and we will obtain from the decay just rate coefficient for ground state ions (we assume they are recombining slower). In Fig. 13 calculated data are plotted in the form used in "advanced analysis." Note that the obtained rate coefficients, given by intercepts of extrapolation of linear parts of the plots with *y*-axis, are insensitive to initial population of excited ions. In stationary afterglow plasma the time of recombination of excited ions will overlap with their formation time and thus the effect of excited ions will probably be reduced. The fact is that we never observed in our experiments the decay, which would indicate the presence of excited ions. This can mean that vibrationally excited ions are quenched within first 10–15 ms, i.e., during formation time. In an afterglow experiment where the decay during first few milliseconds is used for determination of rate coefficients the situation

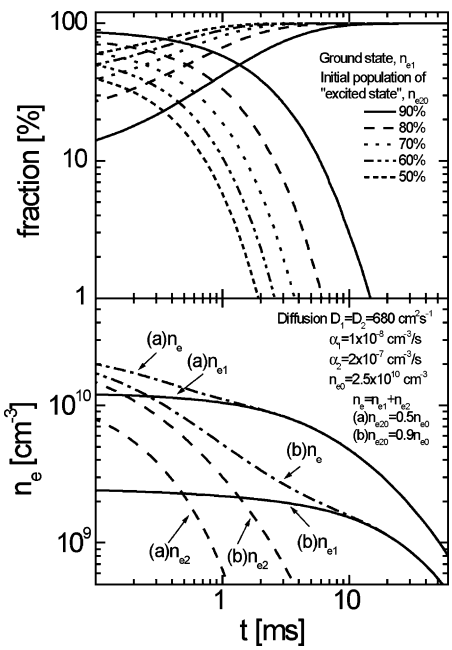

Fig. 12. Upper panel: calculated time evolutions of the relative population of "vibrationally excited" and "ground state" ions during the afterglow. In the calculation it is assumed that ground state ions and vibrationally excited ions recombine with rate coefficients $\alpha_1(v = 0) = 1 \times 10^{-8}\,cm^3\,s^{-1}$ and $\alpha_2(v > 0) = 2 \times 10^{-7}\,cm^3\,s^{-1}$, respectively. The calculations are made for conditions corresponding to present experiment; $p_{He} = 2$ Torr, $n_{e0} = 2.5 \times 10^{10}\,cm^{-3}$. Different lines indicate different initial composition of ions. The diffusion losses are also considered in the calculations. Lower panel: decay of the plasma composed of two ionic species with different rate of recombination. The plots are made for two different initial conditions: (a) $n_{e20} = 0.5n_{e0}$ and (b) $n_{e20} = 0.9n_{e0}$, i.e., for 50 and 90% of excited ions, respectively. Note that in the conditions (a) and (b) excited ions are removed from the plasma by the recombination within <2 and <10 ms, respectively.

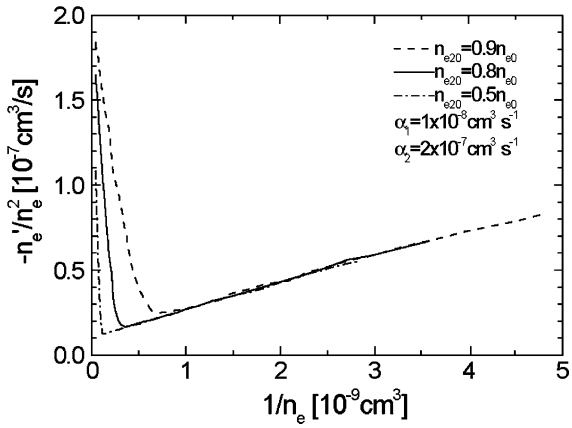

Fig. 13. Advanced analysis—dependence of $(-n_e'/n_e^2)$ vs. $1/n_e$, corresponding to the decay of plasma composed of two ionic species with different rate of recombination. Data are taken from Fig. 12.

can be very different [30–33]. In some storage ring experiments, long relaxation time is used to quench the vibrational excitation, however, the rotational excitation of ions cannot be completely removed in this manner [88]. This is not the case in afterglow experiments because the rotational excitation is quenched very rapidly in multiple collisions with buffer gas atoms.

7. Results

We studied the decay of the afterglow plasma at five different conditions, i.e., with five different dominant ions He_2^+, O_2^+, Ar^+, H_3^+ and D_3^+. In pure He we studied the decay of the plasma containing just He_2^+ ions, in order to determine the diffusion losses and to examine the purity and limitations of the instrument, see Figs. 3 and 4. Decay of plasma with dominant O_2^+ ions and the calibration procedure of the probe was already described in Section 2, see Figs. 5 and 6. By addition of Ar to He we studied the decay of plasma containing just Ar^+ ions; see Figs. 4 and 7. Finally, we studied, in a mixture of He:Ar:H_2, the recombination in plasma containing H_3^+ ions at several pressures of He and several partial pressures of Ar and H_2. Similar study has been made with D_3^+ ions in He:Ar:D_2 mixture. At number densities of H_2 and D_2 higher than $10^{14}\,cm^{-3}$, we studied influence of formation of H_5^+ and D_5^+ on overall de-ionisation process.

The first question which is very obvious is: why mixture of gases He:Ar:H_2 was used? Tu suppress diffusion losses pressure in the discharge chamber has to be over 1 Torr. On another side to avoid formation of H_5^+ low pressure of H_2 have to be used. Using mixture of gasses can satisfy these conditions. Because of proton affinities and high cost of Ne only He and Ar can be used as a buffer gas. To avoid formation of $Ar \times H_3^+$ clusters [89] during the afterglow (see traces in the spectra in Fig. 8) the partial pressure of Ar has to be relatively low, in another words Ar cannot be used as a buffer. The only left possibilities are mixtures He:H_2 and He:Ar:H_2. Both mixtures were used in our early experiments, later in majority of experiments mixture He:Ar:H_2 was used. In this mixture with ~1% of Ar conditions in the discharge are given by He and Ar and H_2 is influencing just afterglow. This separation is not so obvious in He:H_2 and data analysis are more complicated.

7.1. Ar^+ ions

First step in formation of H_3^+ dominated afterglow plasma is the formation of Ar^+ dominated plasma, this formation can be studied in He:Ar mixture. The formation of Ar^+ dominated plasma and measurement of its parameters are already described in Sections 3–5 so only very short summary will be given here.

By flowing 0.2–5 sccm of Ar through the vacuum chamber we obtained, dependent on He flow rate (500–1000 sccm), partial pressure 0.2–5 mTorr of Ar in the discharge chamber. It corresponded to Ar atom density [Ar] ~ $10^{14}\,cm^{-3}$. As it was already mentioned in such mixture Ar^+ and He^+ ions are formed during the microwave pulse. He^+ ions react with He in the three-body association and He_2^+ ions are formed (see Table 2). In the presence of Ar, He_2^+ ions and He^M metastables are converted to Ar^+ in reactions:

$$He_2^+ + Ar \rightarrow Ar^+ + 2He \quad (6)$$

$$He(2^2S, 2^3S) + Ar \rightarrow Ar^+ + He \quad (7)$$

The reaction (7) is very fast (see Table 2) and within 1 ms, the majority of metastables is converted to Ar^+. The charge transfer reaction (6) is also very fast (see Table 2) and also converts majority of He_2^+ to Ar^+. Hence, the rate of the formation of the plasma containing just Ar^+ is given by the formation of He_2^+ in the three-body association of He^+ with He (see Table 2). Examples of Ar^+ decay are plotted in Figs. 4 and 7. Note the perfect linearity of semilogarithmic plot indicating the presence of the fundamental mode diffusion only and the fast completion of formation of plasma containing just Ar^+ ions. This was confirmed also by mass spectrometer (see Fig. 8). We did not observe substantial increase of n_e due to Penning ionisation because this process takes place mostly in the active discharge and within very early phase (<1 ms) of the afterglow. As it was already mentioned it was also

possible, that small number density of Ar metastables was produced; however, that did not cause substantial increase of electron temperature at later afterglow times (see Fig. 7).

The decay of Ar^+ has been regularly re-measured to check for conditions of experiment. The obtained value of ν_D was used to account of the diffusion losses when calculating the recombination rate coefficients of H_3^+ and D_3^+. Observed ν_D was typically by 20% higher than the values calculated for simple cylindrical geometry and actual pressure of He. The reason is very probably partly in the actual inner dimension that is smaller than in the simple geometrical model. The faster decay can also be partly due to reaction of Ar^+ with impurities followed by rapid recombination. The mentioned difference in ν_D, however, was so small that it could be neglected in calculation of α of H_3^+ and D_3^+.

7.2. Recombination of H_3^+

Already from the analyses of the time resolved mass spectra obtained in He–Ar–H_2 mixture (see Figs. 9–11) it is clear that decay of the afterglow plasma depends on partial pressure of H_2. The dependence of a decay of the plasma on value of $[H_2]$ is very strong. Obtained mass spectrometric data are consistent with calculated ionic composition (see Figs. 9–11), nevertheless they can give just qualitative information. The monitoring of the plasma decay by Langmuir probe is required to obtained recombination rate coefficients. As was already demonstrated, at $[H_2] \sim 10^{11}\,cm^{-3}$ formation of H_3^+ is completed within 10–15 ms, at higher $[H_2]$ formation is even faster. We measured decay curves (dependence of electron number density on time) for broad range of pressures of He (1.3–3 Torr) and for very broad range of partial pressures of H_2 (5×10^{10} to $5 \times 10^{15}\,cm^{-3}$). To suppress the level of impurities in used gasses the discharge chamber was cooled down to approx. $-30\,^{\circ}C$. The diffusion losses were also suppressed because of lower temperature.

The examples of obtained decay curves are plotted in the upper panel of Fig. 14. The decay curves

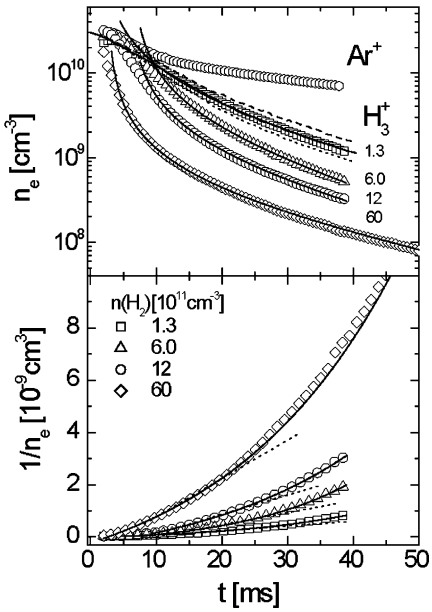

Fig. 14. Upper panel: examples of decay curves, $n_e(t)$, in H_3^+ dominated afterglow obtained at several $[H_2]$. The lines indicate fit of the data by Eq. (2). Upper panel: corresponding $1/n_e$ vs. t plots.

were obtained at different $[H_2]$ with otherwise identical experimental conditions. For higher $[H_2]$ is the decay very fast and it is comparable with decay of O_2^+ dominated plasma, at $[H_2] \sim 10^{11}\,cm^{-3}$ is the decay very slow. The corresponding reciprocal values $1/n_e$ are plotted in the lower panel of Fig. 14. As it was already mentioned the simple solution of balance equation is $1/n_e = 1/n_{e0} + \alpha t$ and the plots should be linear in recombination dominated plasma (doted lines). We were using more general solution given by Eq. (2) to fit the decay curves (indicated by full lines in both panels of Fig. 14). For comparison decay curve obtained for Ar^+ dominated plasma is also included in Fig. 14. The advanced analyse explained above and demonstrated on decay of O_2^+ dominated plasma (see Figs. 5 and 6) was predominantly used to obtain the recombination rate coefficients. The typical plots of values $(-n_e'/n_e^2 - \nu_D/n_e)$ vs. $1/n_e$ obtained in one set of measurements are plotted in Fig. 15. The data are plotted in semilogarithmic scale to cover large range of obtained α_{eff}. The decay curves were analysed

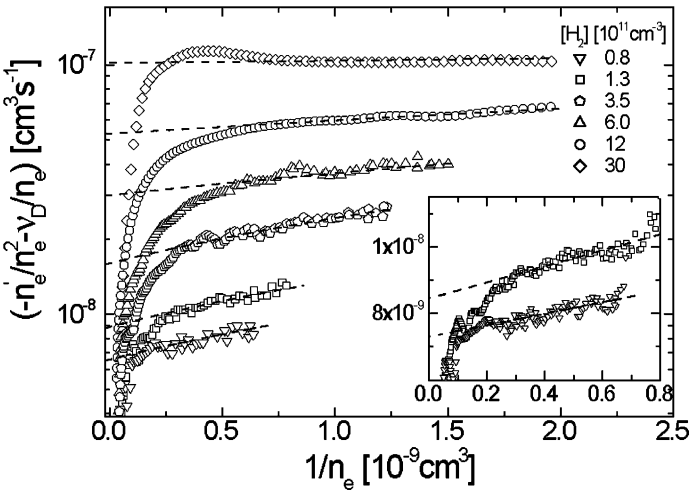

Fig. 15. Advanced analysis—decay of H_3^+ dominated afterglow. Dependence of $(-n'_e/n_e^2 - \nu_D/n_e)$ vs. $1/n_e$ for several values of $[H_2]$. Note that detail in the inset is plotted in linear scale.

together with mass spectrometric data characterised by "*f*" factor (see Figs. 9 and 11). Note in Fig. 15 good fit of the plot by function $\alpha_{\text{eff}} + \nu_R/n$. The plots of fits (dashed lines) are not straight lines because semilogarithmic scale is used. In the inset, the linear scale is used to demonstrate linearity of the plots even at very low $[H_2]$. To ensure proper evaluation of α_{eff}, we made systematic study of the dependence of function $f(t)$ on $[H_2]$. We also realised that from the form of the set of kinetic equations describing formation of H_3^+ from Ar^+ follows that $f(t, [H_2])$ have to fulfil similarity law: $f(t, [H_2]) = f(t/s, s[H_2])$, where s is an arbitrary constant. In another words $f(t, [H_2])$ plotted vs. product $\{t \cdot [H_2]\}$ should be independent on actual $[H_2]$, see the plot in Fig. 16, where data taken from Fig. 11 (upper panel) are replotted. The data obtained from model are also included in Fig. 16. Having information from the analyse of measured and calculated $f(t, [H_2])$ we decided to skip, as a standard, first 5–20 ms of the decay time as a formation time. For $[H_2] > 10^{11}\,\text{cm}^{-3}$ this condition gives $f(t > 20\,\text{ms}) > 0.75$, so for α_{eff} we can write $0.75\alpha < \alpha_{\text{eff}} < \alpha$. Because the measurements are made at least for 60 ms, this is enough to assume that for $[H_2] > 10^{11}\,\text{cm}^{-3}$ values $\alpha_{\text{eff}} \sim \alpha$. For $[H_2] = 0.5\text{–}1 \times 10^{11}\,\text{cm}^{-3}$, the interval for determination of α_{eff} was chosen with the respect to the form of actual function $f(t)$. Because of already mentioned similarity law we believe that in this region obtained value of α_{eff} are not smaller as $\alpha/2$. Values of α_{eff}, obtained during many series of experiments, at pressures of He in the range 1.3–3.0 Torr, are plotted vs. $[H_2]$ in Fig. 17. Extent of He and Ar number densities are also indicated in Fig. 17. Included are previous data of Gougousi et al. [35], Canosa et al. [31,32] and Amano [30]. Temperature of He in these experiments was

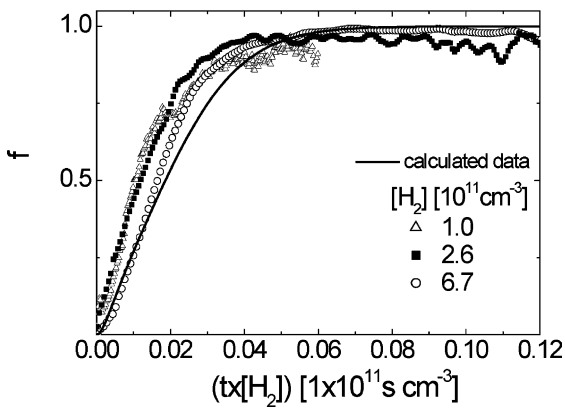

Fig. 16. Similarity law—plot of function $f(t, [H_2])$ vs. product $\{t \cdot [H_2]\}$. The data are taken from Fig. 11. The solid line indicates values obtained from calculated composition as plotted in Fig. 9.

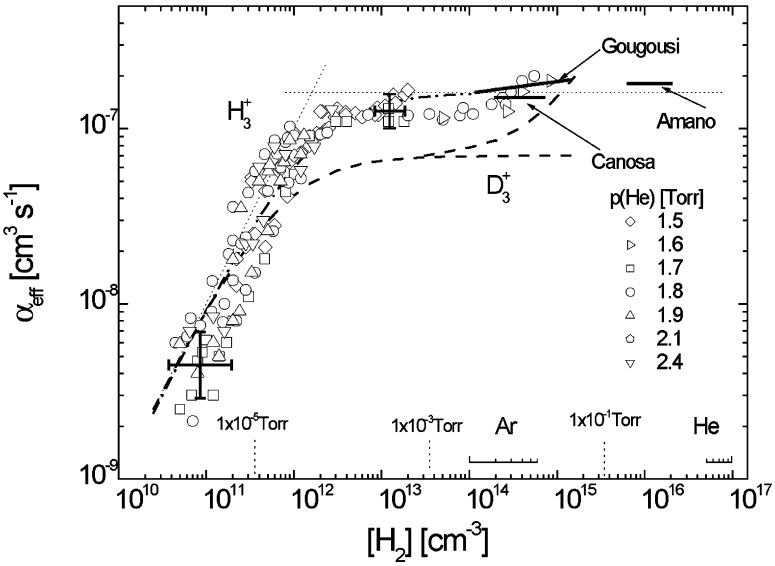

Fig. 17. Recombination of H_3^+; dependence of measured α_{eff} on H_2 number density. Used pressures of He and Ar are indicated. In these experiments He temperature was $\sim 260 \pm 40$ K. Included are also previous results of Gougousi et al. [35], Canosa et al. [32] and Amano [30]. The dashed line indicates the dependence of $\alpha_{eff}(D_3^+)$ on $[D_2]$ corresponding to the recombination of D_3^+ with electrons, see Fig. 21. The crosses indicate estimated error bars.

$\sim 260 \pm 30$ K. The crosses indicate estimated error bars. We carried out many sets of experiments. Every experiment consisted of a pumping and cleaning procedure, tests of the purity and measurements of decay curves at fixed flows of He and Ar and several flows of H_2. Every experiment was finished by further tests of purity to exclude changes during experiment.

We also made systematic study of dependence of α_{eff} on He pressure and on partial pressure of Ar at several values of $[H_2]$. The changing pressures of He and Ar by factor 2–3 we did not find any significant changes of value of α_{eff}. By application of "f correction" to data given in Fig. 17 just points corresponding to $[H_2] = 0.5 \times 10^{11}$ to 1×10^{11} cm^{-3} will be lifted by factor not bigger than 2. Both, advanced analysis (see Eq. (5)) and fit Eq. (2) were used to calculate effective recombination coefficients, no substantial differences were observed. There is no doubt recombination in the afterglow plasma dominated by H_3^+ ions is dependent on partial pressure of hydrogen. This is confirmed by both mass spectrometric data and data obtain by Langmuir probe.

7.3. Recombination of D_3^+

In the mixture of He–Ar–D_2 we measured decay of the plasma dominated by recombination of ions D_3^+ with electrons. Examples of decay curves obtained at several number densities of deuterium are plotted in Fig. 18. Again the decay is very dependent on $[D_2]$. In Fig. 19, the values $(-n_e'/n_e^2 - \nu_D/n_e)$ vs. $1/n_e$ obtained in one set of measurements are plotted. Note the good fit of data by linear function and large range of obtained α_{eff}. In Fig. 20 values $(-n_e'/n_e^2 - \nu_D/n_e)$ and "f" corrected values $(-n_e'/n_e^2 - \nu_D/n_e)/f$ vs. $1/n_e$ are plotted to show difference between α and α_{eff}. Note perfect linearity of "f" corrected plots. The values of α_{eff}, obtained during many series of experiments, at pressures of He in the range 1.3–3.0 Torr, are plotted vs. $[D_2]$ in Fig. 21. Extent of He and Ar number densities are also indicated in Fig. 21. Temperature of He in these experiments was $\sim 230 \pm 40$ K. The crosses indicate estimated error bars. Included are previous data of Laube et al. [57], Gougousi et al. [35].

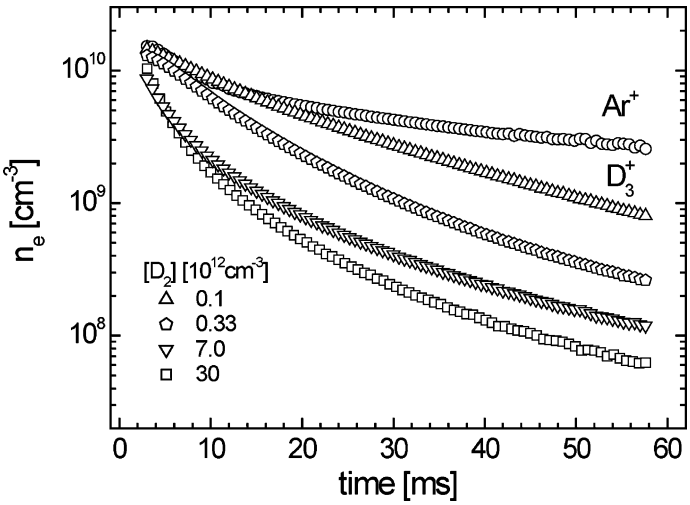

Fig. 18. Examples of decay curves, $n_e(t)$, obtained for several partial pressures of deuterium, in D_3^+ dominated afterglow. The lines indicate fit of the data by Eq. (2).

We considered the possible presence of impurities and their influence on measured data. By measuring decays in pure He and in He with addition of Ar we came to conclusion that the influence of impurities in He and in Ar flow can be neglected when measuring $\alpha > 4 \times 10^{-9}\,\mathrm{cm^3\,s^{-1}}$. For addition of H_2 and D_2 we made their 0.5–3% mixtures with pure He. Mixtures were made from pure gases (grade 5.0, i.e., amount of impurities <10 ppm). Prior to making the mixture, the gases were further purified by flowing via liquid nitrogen trap. Ar was purified by passing via trap with temperature below 210 K. The purity of H_2 was guaranteed sufficiently by its grade; since H_2 partial pressures in mixtures were very small, the level of impurities in H_2 would have to be of the order of several percent to influence the measured recombination—

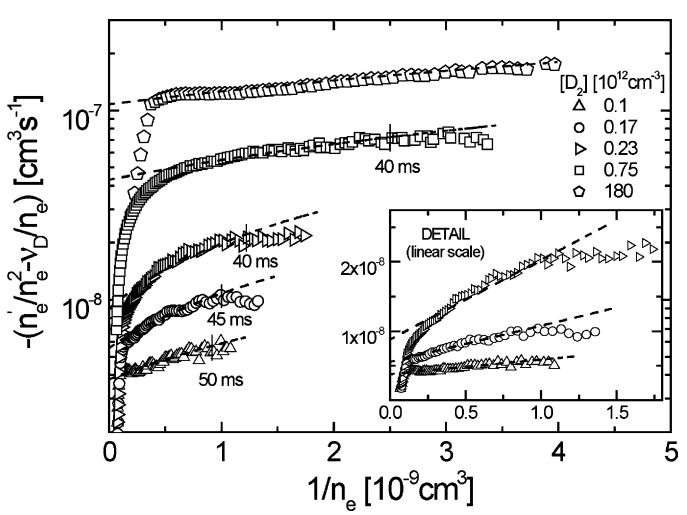

Fig. 19. Advanced analysis—decay of D_3^+ dominated afterglow. Dependence of $(-n_e'/n_e^2 - \nu_D/n_e)$ vs. $1/n_e$ for several values of [D_2]. Note that detail in the inset is plotted in linear scale.

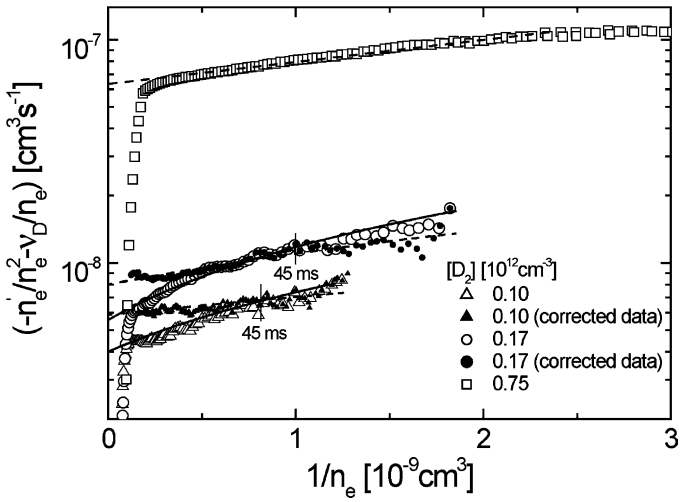

Fig. 20. Advanced analysis including f correction, decay of D_3^+ dominated afterglow. The dependence of $(-n_e'/n_e^2 - \nu_D/n_e)$ vs. $1/n_e$ (open symbols) and "f corrected" values $(-n_e'/n_e^2 - \nu_D/n_e)/f$ vs. $1/n_e$.

and that we can with certainty exclude. The same is true for D_2. Usually the measurement did not take longer than 3 h since we wanted to guarantee the high efficiency of the used liquid nitrogen traps. During this time, we did not observe any "time dependence" of the measured data. Majority of the data was taken with the 0.5 ms microwave pulse width and the repetition period 40–80 ms. Several measurements that

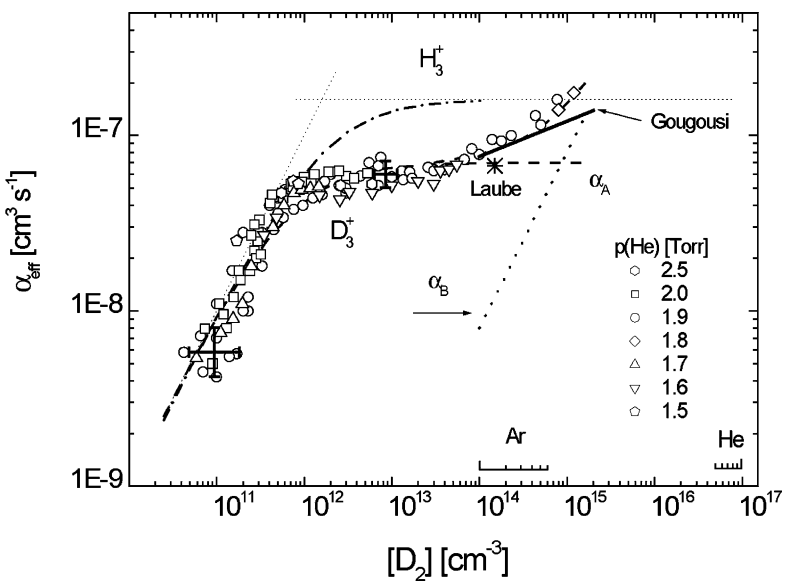

Fig. 21. Recombination of D_3^+; dependence of measured α_{eff} on D_2 number density. Pressures of He and Ar are indicated. In these experiments, He temperature was $\sim 230 \pm 40$ K. Included are also previous results of Laube et al. [57] and Gougousi et al. [35]. The cross indicates estimated error bars. The dash-dotted line indicates the dependence of $\alpha_{eff}(H_3^+)$ on $[H_2]$ corresponding to the recombination of H_3^+ with electrons, see Fig. 19. The straight line labelled as α_B indicates calculated contribution from channel B.

were made with the pulse 2–5 ms long. We repeated the measurements many times during several months in many series of experiments. Prior to the measurements, the vacuum system was baked and pumped for several days. During the studies, we varied orientation of the magnetron antenna, the position and size of the Langmuir probe. We did not detect any problems with the reproducibility of the measured α_{eff}, as long as the measurements of decays of n_e in pure He and He with Ar indicated that the vacuum chamber is clean.

In the mass spectra, we observed traces of ArH_3^+ or ArD_3^+ formed in three-body association with Ar. Because the number density of these ions was very small and we did not observe influence of variation of Ar pressure on observed α_{eff}, we did not consider this ions in data analysis. The presence of these ions in the plasma can just increase decay process and hence increase observed α_{eff}.

Accuracy of obtained α_{eff} is given by the accuracy of instrument calibration (20%) and by the influence of possible impurities. In the measurements of dependence of α_{eff} on $[H_2]$ and [He] accuracy depends also on accuracy of measured flow rates of these gases. We estimated that absolute values of α_{eff} presented in our report are given with accuracy ±50% and the reproducibility (relative accuracy) is ±30%. The scatter of the obtained α_{eff} can also be partly due to variation of temperature of the buffer gas.

8. Discussion

We observe that the effective rate coefficients of recombination of H_3^+ and D_3^+ ions with electrons, α_{eff}, are dependent on $[H_2]$ and $[D_2]$, respectively. We did not observe dependence on He and/or Ar pressure. We stress here once again that we are measuring a rate of recombination in afterglow plasma, which is not necessary, a rate of a binary process. We can make one very important statement at the beginning of this discussion without going to details of the recombination mechanism. Because the binary dissociative recombination is just one of the possible reaction channels that contribute to α_{eff} we can conclude that the rate of binary dissociative recombination, at nearly thermal temperatures is smaller as the lowest value of α_{eff}, of course this can differ for H_3^+ and D_3^+ ions. We can place a limit on values of the rate coefficients of binary dissociative recombination. The rate coefficient for recombination of H_3^+ and D_3^+ ions with electrons are $\alpha_{DR} < 3 \times 10^{-9}\,cm^3\,s^{-1}$ (at ∼260 ± 40 K) and $\alpha_{DR} < 6 \times 10^{-9}\,cm^3\,s^{-1}$ (at ∼230 ± 40 K), respectively. The difference is probably given just by extend of measurements. We cannot say value (number) of α_{DR}, despite the fact that it will be very nice to have it for astronomical calculations [13,15]. We believe that already given limits will cause substantial changes in modelling of ionic composition of interstellar clouds and also in further development of theory of recombination. Further specification of values of α_{DR} will probably require measurements of temperature dependence and evaluation of influence of presence of electrons in decaying plasma on the recombination.

Again, because of similarity of observed phenomena in presence of hydrogen and deuterium we will discuss recombination of H_3^+. At the end we will discuss observed differences between H_3^+ and D_3^+ recombination. Here we will follow discussion, which was given in the Proceeding of ACS Meeting in Chicago 2001 [90]. The dependence of α_{eff} on $[H_2]$ indicates that not only electrons (e^-) and H_3^+ ions but also H_2 molecules participate in the observed de-ionisation process. In general, we can consider two possible mechanisms that differ in the sequence of collisions:

$$\text{A}: \quad H_3^+ + e^- \underset{k_{-1}}{\overset{k_1}{\rightleftarrows}} H_3^* \xrightarrow{k_2[H_2]} \text{neutral products}$$

$$\text{B}: \quad H_3^+ + H_2 \underset{k_{-3}[He]}{\overset{k_3[He]}{\rightleftarrows}} H_5^+ \xrightarrow{\alpha_5[e^-]} \text{neutral products}$$

In channel A first H_3^* is formed in collision of H_3^+ with electron and this is "stabilised' in with H_2. In channel B first H_5^+ is formed in reaction of H_3^+ with H_2 and formed H_5^+ is recombining with electron. Corresponding rate coefficients are indicated in the reaction schema. Because both processes can be considered as independent, the overall rate coefficient

is the sum of the rate coefficients of both channels: $\alpha_{eff} = \alpha_A + \alpha_B$, where α_A and α_B are overall recombination rate coefficients of channel A and B, respectively.

As we will demonstrated below, under our experimental conditions at $[H_2] < 1 \times 10^{13}\,cm^{-3}$ channel B can be neglected and only channel A need to be considered. By application of the steady state approximation [38] we obtain for reaction channel A the following description of the overall effective recombination rate coefficient (see also discussion in [44]):

$$\alpha_A = \frac{k_1 k_2 [H_2]}{k_{-1} + k_2 [H_2]} \quad (8)$$

Here k_1 is the binary rate coefficient of H_3^* formation; k_{-1} is the rate coefficient of unimolecular autoionisation coupled with corresponding lifetime of H_3^*, $\tau_{-1} = 1/k_{-1}$. The binary rate coefficient, k_2, describes the stabilisation processes, here the collisions with H_2. The dash-dotted line plotted in Fig. 17 indicates the fit of measured data by this formula for $[H_2] < 1 \times 10^{13}\,cm^{-3}$, where channel B can be neglected. From the data plotted in Fig. 17 we can see "high-pressure" and "low-pressure" limits (of the channel A) for $k_{-1} < k_2\,[H_2]$ and $k_{-1} > k_2\,[H_2]$, respectively. In the high-pressure limit, we obtain $\alpha_{eff} = \alpha_A = k_1$, i.e., the rate determining process is the formation of H_3^*. The fit of the data gives $k_1 = 1.6 \times 10^{-7}\,cm^3\,s^{-1}$. In the low pressure limit we obtain $\alpha_{eff} = \alpha_A = k_1 k_2 [H_2]/k_{-1}$. From the linearly increasing part of the plot in Fig. 17, we obtained $k_2/k_{-1} = 6 \times 10^{-13}\,cm^3$. From this value, it will be possible to calculate the lifetime of H_3^*, $\tau_{-1} = 1/k_{-1}$, if k_2 can be measured or estimated.

In the similar way, from the plot in Fig. 21, $k_1 = 7 \times 10^{-8}\,cm^3\,s^{-1}$ and $k_2/k_{-1} = 1.5 \times 10^{-12}\,cm^3$ were obtained for recombination of D_3^+. Note that for H_3^+ value of k_1 is approximately two times higher then for D_3^+. The ratios k_2/k_{-1} differ by factor 0.4, higher is the value for D_3^+.

At $[H_2] > 5 \times 10^{13}\,cm^{-3}$ α_{eff} is again increasing with increasing $[H_2]$. Similar increase was observed also for deuterium. To explain the increase of α_{eff}, we considered that the loss of H_3^+ ions proceeds via formation of H_5^+ ion and its successive recombination (scheme B). In the channel B, k_3 is the rate coefficient of the three-body association reaction ($k_3 = 4.6 \times 10^{-30}\,cm^6\,s^{-1}$ at 210 K with H_2 as a third body [22]), and k_{-3} is the rate coefficient for collision-induced dissociation of H_5^+ in collisions with He. The α_5 is the rate coefficient for the recombination of H_5^+ with electrons ($\alpha_5 = 3.6 \times 10^{-6}\,cm^3\,s^{-1}$ see [46]). For loss of H_3^+ we can write: $d[H_3^+]/dt = -\alpha_B [H_3^+][e^-]$; naturally α_B can depend on [He], $[H_2]$ and $[e^-]$. By application of the steady state approximation we obtain:

$$\alpha_B = \frac{k_3}{k_{-3}} \alpha_5 [H_2] \frac{1}{1 + \alpha_5 [e^-]/k_{-3}[He]} \quad (9)$$

From Eq. (9) it follows that the contribution of the channel B is proportional to $[H_2]$ and it is influenced by values of $[e^-]$, [He] (for more details of calculation see [91]). From k_3 and ΔG [92] we calculated (for our experimental conditions) relation: $\alpha_B \sim 8 \times 10^{-23}\,[H_2]\,cm^3\,s^{-1}$, where $[H_2]$ is given in units cm^{-3}. This contribution is identical for hydrogen and for deuterium. The calculated values of α_B relevant to our experiment are indicated by the dotted line in Fig. 21. The calculated α_B is in very good agreement with observed increase of α_{eff} at $[H_2]$, $[D_2] > 5 \times 10^{13}\,cm^{-3}$. Note that α_B can be neglected at $[H_2]$, $[D_2] < 5 \times 10^{13}\,cm^{-3}$. The increase due to the channel B is more pronounced for deuterium because α_A saturates on lower value and at $[D_2] \sim 1 \times 10^{15}\,cm^{-3}$ contributions from both channels are comparable, $\alpha_B = \alpha_A$.

The dependence of α_{eff} smaller on He pressure is negligible particularly in comparison with very strong dependence on partial pressure of H_2. If we realise that the number density of He is six orders of magnitude higher than the number density of H_2, $[He]/[H_2] \approx 10^6$, then the fact that H_2 is more efficient in promoting recombination might seem surprising. There are, however, other examples of such differences in efficiency of stabilisation in kinetics of three-body elementary processes, e.g., the vibrational quenching probability, which varies also over many orders of magnitude in dependence on complex bond energy (see discussion and compilation by Lindinger in [93]).

Now we can look back to Fig. 1 and to Figs. 17 and 1 for results and we can speculate. Majority from re-

cent afterglow experiments measuring recombination of ground state ions were carried out in high-pressure limit of reaction channel A and obtained α_{eff} is equal or close to the rate k_1 (of formation of H_3^*, D_3^*), i.e., they obtained for H_3^+ rate $\sim 2 \times 10^{-7}\,cm^3\,s^{-1}$ [30–32,35], it is in agreement with our results. We can also speculate that if dissociation of H_3^*, D_3^* is enhanced by strong electric field (see, e.g., discussion in [94]) or internal excitation it is possible that "α_{DR}" obtained in some beam experiments is in fact rate of the formation of H_3^*, D_3^*. This can be supported by the observation of the influence of ion source conditions on the measured rate of recombination by Mitchell and co-workers [95].

9. Conclusions

We measured the rate coefficients of the overall recombination of H_3^+ and D_3^+ with electrons (α_{eff}) in decaying plasma with addition of H_2 or D_2, respectively. Since only three-body recombination has been observed we concluded that the binary channels (dissociative recombination) are negligible in our experimental conditions. From our study follows that for astronomy fundamental binary dissociative recombination of H_3^+ ions with electrons is very slow process (at $\sim 260 \pm 40$ K) with rate coefficient $\alpha_{DR} < 3 \times 10^{-9}\,cm^3\,s^{-1}$. For the rate coefficient of dissociative recombination of D_3^+ ions with electrons (at $\sim 230 \pm 40$ K) we obtained limit $\alpha_{DR} < 6 \times 10^{-9}\,cm^3\,s^{-1}$. These results are in accordance with theoretical predictions for the dissociative recombination (see recent [42]). We also made estimation of contribution of "effective recombination" proceeding via formation of H_5^+ (D_5^+) that is only important at large H_2 (D_2) and He densities. This can be important for description of processes in atmospheres of large planets.

Acknowledgements

The authors thank to P. Španìl, D. Smith, J.B.A. Mitchell, N.G. Adams, R. Johnsen, D. Gerlich and M. Lubanski for helpful discussions. In particular we wish to thank to our dear friend late Werner Lindinger for encouraging discussions and support of our work. We thank to the Faculty of Mathematics and Physics that financially supported the construction of AISA in the company Vakuum Praha. Thanks for financial support are due to GACR (202/00/1689, 202/99/D061, 205/02/0610, 202/02/0948), GAUK (146/2000 and 171/2000 B FYZ MFF) and MSM 1132000002. The experiments were carried out with support of EU in frame of the ETR network (HPRN-CT-2000-00142) and with support from EURATOM. The construction of AISA was supported in part by the VW foundation (Schwerpunkt Intra- and inter-moleculare Electronenubertragung, Az.: I/72 593).

References

[1] D. Smith, P. Španěl, Mass Spectrom. Rev. 14 (1995) 255.
[2] B.J. McCall, R. Geballe, K.H. Hinkle, T. Oka, Science 279 (1998) 1910.
[3] A. Dalgarno, Adv. Atom. Mol. Opt. Phys. B 32 (1994) 57.
[4] D. Uy, M. Cordonnier, T. Oka, Phys. Rev. Lett. 78 (20) (1997) 3844.
[5] T.R. Geballe, T. Oka, Nature 384 (6607) (1996) 334.
[6] T. Oka, in: M. Larson, J.B.A. Mitchell, I.F. Schneider (Eds.), Dissociative Recombination, Theory, Experiment and Applications IV, World Scientific, Singapore, 1999, p. 131.
[7] A. Dalgarno, in: M. Larson, J.B.A. Mitchell, I.F. Schneider (Eds.), Dissociative Recombination, Theory, Experiment and Applications IV, World Scientific, Singapore, 1999, p. 1.
[8] E. Herbst, Phys. Trans. R. Soc. Lond. A 358 (2000) 2523.
[9] T.R. Geballe, M.F. Jagod, T. Oka, Astrophys. J. 408 (1993) L109.
[10] J.E.P. Connerney, T. Satoh, Phys. Trans. R. Soc. Lond. A 358 (2000) 2471.
[11] M. Larsson, Phys. Trans. R. Soc. Lond. A 358 (2000) 2433.
[12] A.E. Orel, I.F. Schneider, A. Suzor-Weiner, Phys. Trans. R. Soc. Lond. A 358 (2000) 2445.
[13] T. Oka, Abstract paper, Am. Chem. S 222: U208–U208, Part 2, 2001.
[14] C.H. Greene, V. Kokoouline, B.D. Esry, Abstract paper, Am. Chem. S 222: U208–U208, Part 2, 2001.
[15] B.J. McCall, Abstract paper, Am. Chem. S 222: U208–U208, Part 2, 2001.
[16] R.K. Janev, in: M. Larsson, J.B.A. Mitchell, I.F. Schneider (Eds.), Proceedings of the 1999 Conference on Dissociative Recombination, Theory, Experiment and Applications IV, World Scientific, Singapore, 1999.
[17] Y. Ikezoe, S. Matsuoka, M. Takebe, A. Viggiano, Gas Phase Ion–Molecule Reaction Rate Constants, The Mass Spectroscopy Society of Japan, Tokyo, 1987.

[18] V.G. Anicich, J. Phys. Chem. Ref. Data 22 (1993) 1469.
[19] J. Glosík, Int. J. Mass Spectrom. Ion Process. 139 (1994) 15.
[20] B.M. Smirnov, Complex Ions, Nauka, Moscow, 1984.
[21] T. Glenewinkel-Meyer, D. Gerlich, Isr. J. Chem. 37 (1997) 343.
[22] R. Johnsen, C.-M. Huang, M.A. Biondi, J. Chem. Phys. 65 (1976) 1539.
[23] A. Aguado, O. Roncero, C. Tablero, C. Sanz, M. Paniagua, J. Chem. Phys. 112 (2000) 1240.
[24] M.A. Biondi, S.C. Brown, Phys. Rev. 76 (1949) 1697.
[25] J.M. Richardson, R.B. Holt, Phys. Rev. 81 (1951) 153.
[26] L.J. Varnerin Jr., Phys. Rev. 84 (1951) 563.
[27] K.B. Persson, S.C. Brown, Phys. Rev. 100 (1955) 729.
[28] N.G. Adams, D. Smith, E. Alge, J. Chem. Phys. 81 (1984) 1778.
[29] M.R. Flannery, in: I. Alvarez, C. Cisneros, T.J. Morgan (Eds.), Atomic and Molecular Physics, World Scientific, London, 1995, p. 329.
[30] T. Amano, J. Chem. Phys. 92 (1990) 6492.
[31] A. Canosa, B.R. Rowe, J.B.A. Mitchell, J.C. Gomet, C. Rebrion, Astron. Astrophys. 248 (1991) L19.
[32] A. Canosa, J.C. Gomet, B.R. Rowe, J.B.A. Mitchell, J.L. Queffelec, J. Chem. Phys. 97 (1992) 1028.
[33] D. Smith, P. Španěl, Int. J. Mass Spectrom. Ion Process. 129 (1993) 163.
[34] D. Smith, P. Španěl, Chem. Phys. Lett. 211 (1993) 454.
[35] T. Gougousi, R. Johnsen, M.F. Golde, Int. J. Mass Spectrom. Ion Process. 149/150 (1995) 131.
[36] B.J. McCall, R. Geballe, K.H. Hinkle, T. Oka, Astrophys. J. 522 (1999) 338.
[37] B.J. McCall, K.H. Hinkle, R. Geballe, G.H. Moriarty-Schieven, N.J. Evans II, K. Kawaguchi, S. Tokano, V.V. Smith, T. Oka, Astrophys. J. 567 (2002) 391.
[38] P.W. Atkins, Physical Chemistry, 3rd Edition, Oxford University Press, London, 1988.
[39] T.I.F. Schneider, M. Larson, A.E. Orel, A. Suzor-Weiner, in: M. Larson, J.B.A. Mitchell, I.F. Schneider (Eds.), Dissociative Recombination, Theory, Experiment and Applications IV, World Scientific, Singapore, 1999, p. 131.
[40] T. Tanabe, K. Chida, T. Watanabe, Y. Arakaki, H. Takagi, I. Katayama, Y. Haruyama, M. Saito, I. Nomura, T. Honma, K. Noda, K. Hoson, in: M. Larson, J.B.A. Mitchell, I.F. Schneider (Eds.), Dissociative Recombination, Theory, Experiment and Applications IV, World Scientific, Singapore, 1999, p. 170.
[41] I.F. Schneider, A.E. Orel, A. Suzur-Weiner, Phys. Rev. Lett. 85 (2000) 3785.
[42] V. Kokoouline, C.H. Greene, B.D. Esry, Nature 412 (2001) 891.
[43] J. Glosík, R. Plašil, V. Poterya, P. Kudrna, M. Tichý, Chem. Phys. Lett. 331 (2000) 209.
[44] J. Glosík, R. Plašil, V. Poterya, P. Kudrna, M. Tichý, A. Pysanenko, J. Phys. B: Atom. Mol. Opt. Phys. 34 (2001) L485.
[45] V. Poterya, J. Glosík, R. Plašil, M. Tichý, P. Kudrna, A. Pysanenko, Phys. Rev. Lett. 88 (2002) 044802-1.
[46] M.T. Leu, M.A. Biondi, R. Johnsen, Phys. Rev. A 8 (1973) 413.
[47] B. Peart, K.T. Dolder, J. Phys. B 7 (1974) 1948.
[48] D. Auerbach, R. Cacak, R. Caudano, T.D. Gaily, C.J. Keyser, J.Wm. McGowan, J.B.A. Mitchell, S.F.J. Wilk, J. Phys. B 10 (1977) 3797.
[49] D. Mathur, S.U. Khan, J.B. Hasted, J. Phys. B 11 (1978) 3615.
[50] J.W.M. McGowan, P.M. Mul, V.S. D'Angelo, J.B.A. Mitchell, P. Defrance, H.R. Froelich, Phys. Rev. Lett. 42 (1978) 373.
[51] J.A. MacDonald, M.A. Biondi, R. Johnsen, Planet Space Sci. 32 (1984) 651.
[52] N.G. Adams, D. Smith, in: J.B.A. Mitchell, S.L. Guberman (Eds.), Dissociative Recombination, Theory, Experiment and Application, World Scientific, Singapore, 1989, p. 29.
[53] H. Hus, F. Sen, A. Jousif, J.B.A. Mitchell, Phys. Rev. A 38 (1988) 658.
[54] M. Feher, A. Rohrbacher, J.P. Maier, Chem. Phys. 185 (1994) 357.
[55] G. Sundström, J.R. Mowat, H. Danared, S. Datz, L. Broström, A. Filevich, A. Källberg, S. Mannervik, K.G. Rensfeld, P. Sigray, M. Af Ugglas, M. Larson, Science 263 (1994) 785.
[56] M. Larson, Int. J. Mass Spectrom. Ion Process. 149/150 (1995) 403.
[57] S. Laube, et al., J. Phys. B: Atom. Mol. Opt. Phys. 31 (1998) 2111.
[58] P. Kudrna, R. Plašil, J. Glosík, M. Tichý, V. Poteriya, J. Rusz, Czech J. Phys. 50 (S3) (2000) 329.
[59] M.J. Jehnsen, H.B. Pederson, C.P. Safvan, K. Seiersen, X. Urbain, L.H. Andersen, Phys. Rev. A 6305 (2001) 2701.
[60] M. Larsson, H. Danared, A. Larson, P. Le, J.R. Peterson, S. Rosen, J. Semeniak, C. Stromholm, Phys. Rev. Lett. 79 (1997) 395.
[61] P. Le, M. Larsson, H. Danared, A. Larson, J.R. Peterson, S. Rosen, J. Semeniak, C. Stromholm, Phys. Scripta 57 (1998) 215.
[62] J. Glosík, P. Zakouřil, V. Hanzal, V. Skalský, Int. J. Mass Spectrom. Ion Process. 149/150 (1995) 187.
[63] R. Plašil, P. Zakouřil, J. Glosík, J. Phys. B: Atom. Mol. Opt. Phys. 32 (1999) 3575.
[64] D. Smith, I.C. Plumb, J. Phys. D: Appl. Phys. 5 (1972) 1226.
[65] D. Smith, Planet Space Sci. 20 (1972) 1717.
[66] A.G. Dean, D. Smith, I.C. Plumb, J. Phys. E (Sci. Instrum.) 5 (1992) 776.
[67] B.M. Wunderer, J. Phys. E (Sci. Instrum.) 8 (1975) 938.
[68] J.D. Swift, M.J.R. Schwar, Electrical Probes for Plasma Diagnostics, Iliffe, London, 1970.
[69] J. Glosík, G. Bano, R. Plašil, A. Luca, P. Zakouřil, Int. J. Mass Spectrom. 189 (1999) 103.
[70] O. Chudáček, P. Kudrna, H. Miler, M. Brzobohatý, M. Tichý, in: J. Píchal (Ed.), Proceedings of the 17th Symposium on Plasma Physics and Technology, Prague (Czech Republic), 13–16 June 1995, p. 221.
[71] R. Deloche, P. Monchicourt, M. Cheret, F. Lambert, Phys. Rev. A 13 (1976) 1140.
[72] A.V. Phelps, Phys. Rev. 82 (1955) 453.

[73] X. Urbain, in: M. Larson, J.B.A. Mitchell, I.F. Schneider (Eds.), Dissociative Recombination, Theory, Experiment and Applications IV, World Scientific, Singapore, 1999, p. 131.
[74] L. Talbot, Y.S. Chou, Rarefied Gas Dynamics, Academic Press, New York, 1966, p. 1723.
[75] O. Chudáček, P. Kudrna, J. Glosík, M. Šícha, M. Tichý, Contrib. Plasma Phys. 35 (1995) 503.
[76] R. Johnsen, Int. J. Mass Spectrom. Ion Process. 81 (1987) 67.
[77] P. Španěl, L. Dittrichová, D. Smith, Int. J. Mass Spectrom. Ion Process. 129 (1993) 183.
[78] E.W. McDaniel, J.B.A. Mitchell, M.E. Rudd, Atomic Collisions, Heavy Particles Projectiles, Wiley/Interscience, New York, 1993.
[79] D. Trunec, P. Španěl, D. Smith, Contrib. Plasma Phys. 34 (1994) 69.
[80] M.J. Druyvesteyn, Z. Phys. 64 (1930) 781.
[81] M. Šícha, J. Glosík, J. Pavlík, Z. Nemeček, J. Šafranková, M. Tichý, Czech J. Phys. B 33 (1983) 1226.
[82] A. Savitzky, M.J.E. Golay, Anal. Chem. 36 (1964) 1627.
[83] M. Tichý, P. David, M. Šícha, D. Trunel, Contrib. Plasma Phys. 34 (1994) 59.
[84] P. Kudrna V. Poterya, J. Glosík, R. Plašil, A. Pysanenko, M. Tichý, Czeck J. Phys. (2002), in press.
[85] I. Dotan, W. Lindinger, J. Chem. Phys. 76 (1982) 4972.
[86] H. Villinger, J.H. Futrell, F. Howorka, N. Duric, W. Lindinger, J. Chem. Phys. 76 (1982) 3529.
[87] B.K. Chatterjee, R. Johnsen, J. Chem. Phys. 93 (1990) 5681.
[88] M. Larsson, Private communication (2001).
[89] M. Kaczorovska, S. Roszak, J. Leszcynski, J. Phys. Chem. 105 (2001) 7938.
[90] J. Glosík, Abstract paper, Am. Chem. S 222: U208–U208, Part 2, 2001.
[91] J. Glosík, R. Plašil, V. Poterya, A. Pysanenko, Czech J. Phys. 2002, in press.
[92] K. Hiraoka, T. Mori, Chem. Phys. Lett. 157 (1989) 467.
[93] W. Lindinger, Int. J. Mass Spectrom. Ion Process. 80 (1987) 115.
[94] E.W. McDaniel, J.B.A. Mitchell, M.E. Rudd, Atomic Collisions, Heavy Particle Projectiles, Wiley, New York, 1993.
[95] P. Van der Donk, F.B. Yousif, J.B.A. Mitchell, Phys. Rev. A 43 (1991) 6573.